Vegetation response to precipitationvariability in East Africa controlled by biogeographical factors

Hawinkel, P.; Thiery, Wim; Lhermitte, Stef; Swinnen, E.; Verbist, B.; Van Orshoven, J.; Muys, B.

Important note
To cite this publication, please use the final published version (if applicable).
Please check the document version above.

Key Points:
- East African ecosystems respond to varying extents to interannual climate variability
- Mean annual precipitation, vegetation type, and ocean-climate coupling control this relationship
- Additive modeling with spatiotemporal data products reveals the critical role of data uncertainty

Correspondence to:
P. Hawinkel and B. Muys,
pieterhawinkel@gmail.com;
bart.muys@ees.kuleuven.be

Vegetation response to precipitation variability in East Africa controlled by biogeographical factors

P. Hawinkel[1,2], W. Thiery[3], S. Lhermitte[4], E. Swinnen[1], B. Verbist[2], J. Van Orshoven[2], and B. Muys[2]

[1]Flemish Institute for Technological Research (VITO), Remote Sensing Unit, Mol, Belgium, [2]Department of Earth and Environmental Sciences, KU Leuven–University of Leuven, Leuven, Belgium, [3]ETH Zürich, Institute for Atmospheric and Climate Science, Land-Climate Dynamics, Zürich, Switzerland, [4]Delft University of Technology, Department of Geoscience & Remote, Sensing, Delft, Netherlands

Abstract Ecosystem sensitivity to climate variability varies across East Africa, and identifying the determinant factors of this sensitivity is crucial to assessing region-wide vulnerability to climate change and variability. Such assessment critically relies on spatiotemporal data sets with inherent uncertainty, on new processing techniques to extract interannual variability at a priori unknown time scales and on adequate statistical models to test for biogeographical effects on vegetation-precipitation relationships. In this study, interannual variability in long-term records of normalized difference vegetation index and satellite-based precipitation estimates was detected using ensemble empirical mode decomposition and standardized precipitation index with varying accumulation periods. Environmental effect modeling using additive models with spatially correlated effects showed that ecosystem sensitivity is primarily predicted by biogeographical factors such as annual precipitation distribution (reaching maximum sensitivity at 500 mm yr^{-1}), vegetation type and structure, ocean-climate coupling, and elevation. The threat of increasing climate variability and extremes impacting productivity and stability of ecosystems is most imminent in semiarid grassland and mixed cropland ecosystems. The influence of oceanic phenomena such as El Niño–Southern Oscillation and Indian Ocean Dipole is foremost reflected in precipitation variability, but prolonged episodes also pose risks for long-term degradation of tree-rich ecosystems in the East African Great Lakes region.

1. Introduction

Terrestrial ecosystems respond to fluctuations in climatic conditions, which are primarily measured as interannual variability in precipitation and temperature regimes [*Myoung et al.*, 2013]. Climate-driven inter-annual vegetation changes affect ecosystem services such as carbon sequestration in soil and biomass [*Luyssaert et al.*, 2007; *Piao et al.*, 2011], water cycle regulation [*Hirabayashi et al.*, 2013; *Liu et al.*, 2008], and rain-fed crop production [*Cooper et al.*, 2008; *Knox et al.*, 2012; *Ray et al.*, 2015]. Empirical studies have demonstrated greening and browning responses of ecosystem photosynthetic activity due to increased interannual climate variability [*De Keersmaecker et al.*, 2015; *Holmgren et al.*, 2013].

Viewed on a subcontinental scale, interannual vegetation response is spatially heterogeneous due to variations in mesoscale climate [*Plisnier et al.*, 2000], mean annual precipitation [*Camberlin et al.*, 2007; *Greve et al.*, 2011], and topographic factors [*White et al.*, 2005]. Understanding these interactions is key to making spatial projections of the impacts of climate change on natural and managed ecosystems, delineating vulnerable areas, and implementing adaptation and mitigation measures [*Intergovernmental Panel on Climate Change*, 2014].

Semiarid ecosystems in Africa have been identified as particularly vulnerable to the impacts of increased climate variability [*Busby et al.*, 2014]. As opposed to the well-studied Sahel region [e.g., *Dardel et al.*, 2014; *Fensholt et al.*, 2013; *Herrmann et al.*, 2005; *Nicholson*, 2013; *Nicholson et al.*, 1990], East Africa represents a specific case where strong topographic effects, exposure to oceanic influence, and strong heterogeneity of vegetation types contribute to the uncertainty on the fate of ecosystems under changing climate conditions. To date, regional assessments of ecosystem response to climate variability [e.g., *Brando et al.*, 2010; *Brown et al.*, 2010; *Guo et al.*, 2014; *Ibrahim et al.*, 2015; *Ivits et al.*, 2014] face unresolved challenges in terms of data consistency, time series analysis techniques, and statistical modeling approaches.

First, consistency in spatiotemporal data sets for long-term ecosystem studies is a subject of current research. In remote sensing-based vegetation monitoring, the key issue is temporal consistency and calibration between subsequent sensors to minimize spurious temporal trends [e.g., *Gonsamo and Chen*, 2013; *Nagol*

et al., 2014; *Tian et al.*, 2015]. As for climatic records, the main challenge in obtaining spatially consistent data products is to trade off the spatial density of observations against the uncertainty of the models and algorithms [e.g., *Awange et al.*, 2016; *Maidment et al.*, 2013; *Sapiano*, 2010], particularly in data-scarce regions. Often, ecosystem sensitivity studies tend to draw conclusions from one particular combination of vegetation and climate data sets without accounting for the potential effects of data inconsistency.

Second, interannual variability of vegetation greenness is a key variable for assessing ecosystem responses to climatic change and variability [*Hilker et al.*, 2014; *Luo et al.*, 2011]. Separating interannual variability from annual variability requires dedicated temporal filtering tools for time series. A wide range of time series decomposition tools have been reported, based on parameterization of growing seasons [*Eerens et al.*, 2014; *Jönsson and Eklundh*, 2002], Fourier analysis [e.g., *Immerzeel et al.*, 2005; *Lhermitte et al.*, 2008], trend and break detection [*Verbesselt et al.*, 2010], principal component analysis [*Ivits et al.*, 2014; *Myoung et al.*, 2013], wavelet decomposition [*Martínez and Gilabert*, 2009; *Swinnen*, 2008; *Torrence and Compo*, 1998], or empirical mode decomposition (EMD) [*Hawinkel et al.*, 2015; *Huang et al.*, 1998; *Wu and Huang*, 2009]. Despite this abundance of techniques, it has not yet been shown how these can provide a meaningful spatial indicator of interannual response to climate variability over large spatial scales.

A third challenge toward understanding sensitivity of ecosystems to climate variability is to identify the biogeographical factors controlling this response, which can be either topographic, ecological, meteorological, or related to the regional climate-ocean interactions. Whereas early approaches were merely descriptive [e.g., *Braswell et al.*, 1997; *Camberlin et al.*, 2007; *Farrar et al.*, 1994; *Nicholson and Farrar*, 1994], recent studies have used explanatory statistical techniques to evaluate the role of biogeographical factors by hypothesis testing [*Brown et al.*, 2010], linear regression techniques [*Li et al.*, 2013; *Zhao et al.*, 2015], nonlinear relationships [*White et al.*, 2005], and mixed-effect modeling with spatial correlation [*De Jong et al.*, 2013]. However, systematic assessment of ecosystem sensitivity to climate variability still lacks a unified statistical approach. A consistent set of techniques to deal with multiple, nonlinear, and spatially correlated effects through hypothesis testing have already been explored in environmental effect modeling of biological systems [*Zuur et al.*, 2009].

Therefore, the objectives of this research are threefold. First, we systematically consider the impacts of spatiotemporal data uncertainty in a regional study of ecosystem sensitivity to climate variability. Second, we aim to quantify and map the interannual response of East African ecosystems to climate variability from various spatiotemporal data sets. The third objective of this paper is to fully integrate environmental effect modeling into spatiotemporal assessments of interannual ecosystem responses to climate variability, applied to East Africa.

First, an overview of the current knowledge on East Africa's climate dynamics is given. Also, the crucial issue of uncertainty in spatiotemporal data products is discussed prior to the selection of cross-sensor vegetation index time series and satellite-based spatial precipitation estimates. Next, we employ a novel time series decomposition tool based on ensemble empirical mode decomposition (EEMD) to extract and map the interannual vegetation response to precipitation variability over East Africa. Finally, an environmental effect model is presented to identify and quantify the biogeographical factors that determine the vegetation response to interannual climate variability (i.e., precipitation patterns, ocean-coupled phenomena such as El Niño–Southern Oscillation (ENSO) and Indian Ocean Dipole (IOD), topographic parameters, and vegetation structure).

The results contribute significantly to the quantitative knowledge of the sensitivity of East African ecosystems to climate variability and of its controlling factors and help to delineate vulnerable areas under future climate scenarios of increased variability. Also, they serve to demonstrate and evaluate a systematic analysis framework for regional climate sensitivity studies worldwide.

2. Study Area

The ecosystems of East Africa (hereafter defined as the region spanning 26.4°E to 51.4°E and 14.7°N to 12.0°S) are strongly determined by the distinct regional topography, their tropical latitude, and the proximity of the Indian Ocean as shown in Figure 1. The eastern and western branches of the East African Rift System consist of chains of extensional basis which form the East African Great Lake and are lined with volcanic highlands.

Annual rainfall variability in East Africa is dominated by the seasonal migration of the Intertropical Convergence Zone (ITCZ), which induces a strong periodic cycle of precipitation [*Anyah and Semazzi*, 2006, 2007]. Two rainy seasons are associated with the passage of the ITCZ, i.e., "long rains" from March to May
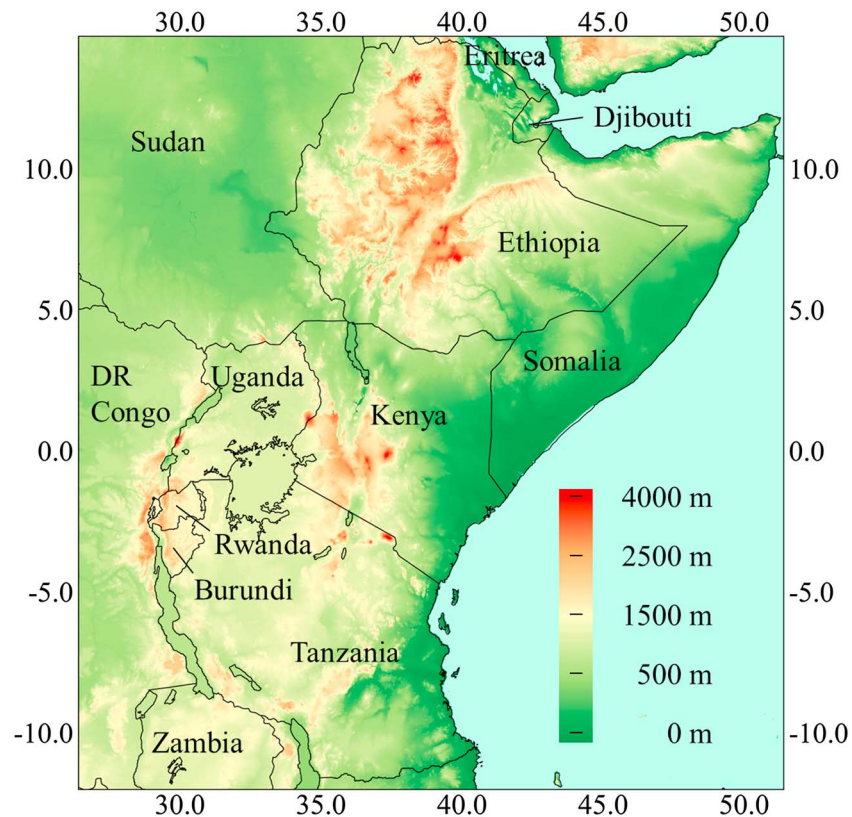
Figure 1. Elevation map of East Africa (GTOPO30).

and "short rains" from October to December, interrupted by a major dry season from June to August [*Anyah and Semazzi*, 2006; *Philippon et al.*, 2015].

On the interannual time scale, precipitation variability over East Africa is large in terms of magnitude as well as timing [*Kizza et al.*, 2009], with the short rains displaying stronger interannual variability than the long rains [*Behera et al.*, 2005]. Interannual precipitation variability is generally attributed to annual-to-decadal oscillations of sea surface temperatures (SSTs) that influence the large-scale continental climate. The teleconnections known to act over East Africa are IOD [*Saji et al.*, 1999] and ENSO [*Ropelewski and Halpert*, 1987; *Trenberth*, 1997]. In particular, most of the interannual variability during the short rains as well as other seasons has been linked to IOD [*Behera et al.*, 2005; *Black et al.*, 2003; *Conway et al.*, 2007; *Lanckriet et al.*, 2015; *Marchant et al.*, 2007; *Omondi et al.*, 2013; *Williams and Funk*, 2011; *Zaroug et al.*, 2014]. Several studies have also found the imprint of ENSO on the variability of the short rains over parts of East Africa [*Giannini et al.*, 2008; *Indeje et al.*, 2001; *Plisnier et al.*, 2000; *Schreck and Semazzi*, 2004; *Segele et al.*, 2009; *Smith and Semazzi*, 2014; *Sun et al.*, 1999].

Besides this oceanic forcing of East African climate, the characteristics of the land surface play an important role in modulating precipitation across this region. In particular, evaporation from vegetation or lakes [*Akkermans et al.*, 2014; *Spracklen et al.*, 2012; *Thiery et al.*, 2014a, 2014b], heat flux regulation by soil moisture fluxes [*Guillod et al.*, 2015; *Taylor et al.*, 2012], orographic lifting processes [*Anyah and Semazzi*, 2007; *Laing et al.*, 2011], and initiation of mesoscale circulation by land-water contrasts [e.g., *Anyah et al.*, 2006; *Ba and Nicholson*, 1998; *Laing et al.*, 2011; *Lauwaet*, 2009] are key local drivers of precipitation production over East Africa.

A wide range of ecological zones and associated vegetation types occurs (Figure 2), largely oriented along the precipitation gradient (Figure 3). West of the East African Rift, latitudinal bands of mean annual precipitation determine the transition from tropical forest and woodland systems to shrub- and grass-dominated savannah systems. Along the rift, topography creates climatic gradients that result in distinct Afromontane forests in Ethiopia, Kenya, and Rwanda with their associated agroforestry systems. East of the rift, arid and semiarid conditions impose grassland savannah, sparse shrubland, and thicket vegetation in the lowlands
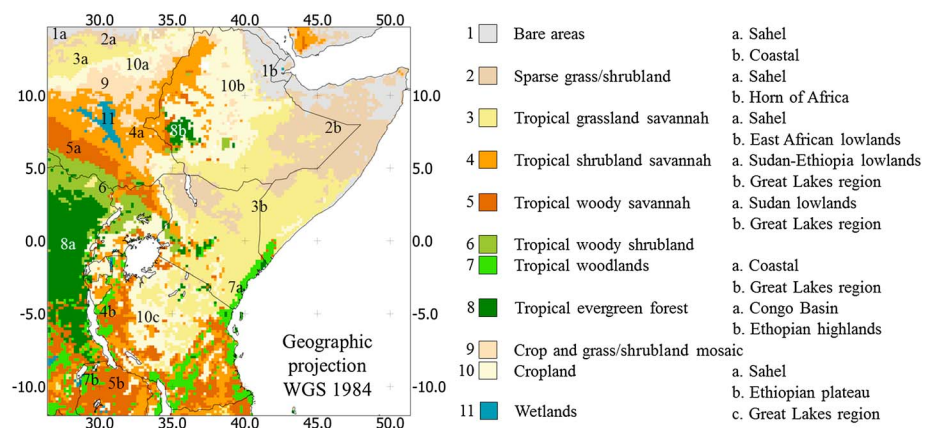
Figure 2. Ecological zones of East Africa as derived from Global Land Cover 2000 (GLC2000) [*Bartholomé and Belward*, 2005] represent land cover types in distinct climatological and topographical regions at 20 km spatial resolution.

of Somalia, eastern Ethiopia, and Kenya [*Lillesø et al.*, 2011], allowing pastoral grazing activities. Mixed cereal cropping systems prevail in the subhumid and humid parts of the plateau around Lake Victoria (stretching eastern Kenya, Tanzania, Burundi, Rwanda, and Uganda) and in the Ethiopian Highlands. The starting hypothesis is that vegetation response to precipitation variability is most distinct between ecological zones, since vegetation structure and its photosynthetic capacity are the primary limiting factors for gross canopy photosynthesis across semiarid (250–500 mm yr^{-1}) and subhumid (500–900 mm yr^{-1}) Africa [*Williams et al.*, 2008]. Precipitation gradients within those zones are put forward as the controlling factor of this response. Important deviations from this pattern are expected in areas with strong orography, i.e., the Ethiopian Highlands and the rims of the East African Rift valley. Finally, although the effects of ENSO and IOD on precipitation variability are well studied, it is unknown if and how this ocean-climate coupled forcing translates into alterations of the interannual vegetation response.

3. Data

3.1. Normalized Difference Vegetation Index Data Sets

Satellites with optical multispectral sensors in a near-polar orbit provide periodic images in visible and infrared wavelengths. The normalized difference vegetation index (NDVI) [*Tucker and Sellers*, 1986] is an indicator of the photosynthetic activity and the greenness of vegetation. It is calculated per pixel from red (R) and infrared (NIR):

$$NDVI = (Refl_{NIR} - Refl_{R})/(Refl_{NIR} + Refl_{R}) \qquad (1)$$

The NDVI produced from historical satellite image archives (as from 1979 with NOAA-advanced very high resolution radiometer (AVHRR) [*Cracknell*, 2001]) captures the long-term responses of ecosystems to climate variability [*Dubovyk et al.*, 2012; *Pettorelli et al.*, 2005; *Yengoh et al.*, 2014]. However, a critical step when integrating the temporal NDVI trajectories from different sources is to account for artifacts in one-sensor data series (e.g., volcanic eruptions and platform orbital drift [*Nagol et al.*, 2014; *Swinnen et al.*, 2014]) and between-sensor inconsistencies due to differences in Sun-target-sensor geometry [*Swinnen and Veroustraete*, 2008], sensor spectral response [*Trishchenko et al.*, 2002], or processing specifications [*Tian et al.*, 2015].

Efforts to minimize these uncertainties and maximize temporal consistency have resulted in cross-sensor data products such as the 15 day composite NDVI product of the Global Inventory Modeling and Mapping Studies (GIMMS3g) [*Fensholt and Proud*, 2012]; NASA's Long-Term Data Record (LTDR v4) [*NASA*, 2014]; the continuum of SPOT-VGT1, VGT2, and PROBA-V products [*Deronde et al.*, 2014; *Dierckx et al.*, 2014; *Swinnen et al.*, 2014]; and the higher spatial resolution NDVI record of shorter length from the Moderate Resolution Imaging Spectroradiometer instrument [*Huete et al.*, 2002]. For a quantitative comparison of these data sets for long-term temporal analysis, we refer to *Tian et al.* [2015]. Based on their analysis, the newly updated GIMMS3g data set [*Fensholt and Proud*, 2012] can be considered the state-of-the-art global consistent long-term NDVI record for spatiotemporal analysis (R. Fensholt, personal communication, 2 October 2015). GIMMS3g consists of recalibrated historic NOAA-AVHRR data (0.083° resolution, 1981–2011) and corrects for spurious trends due to calibration loss, volcanic eruptions, and orbital drift.
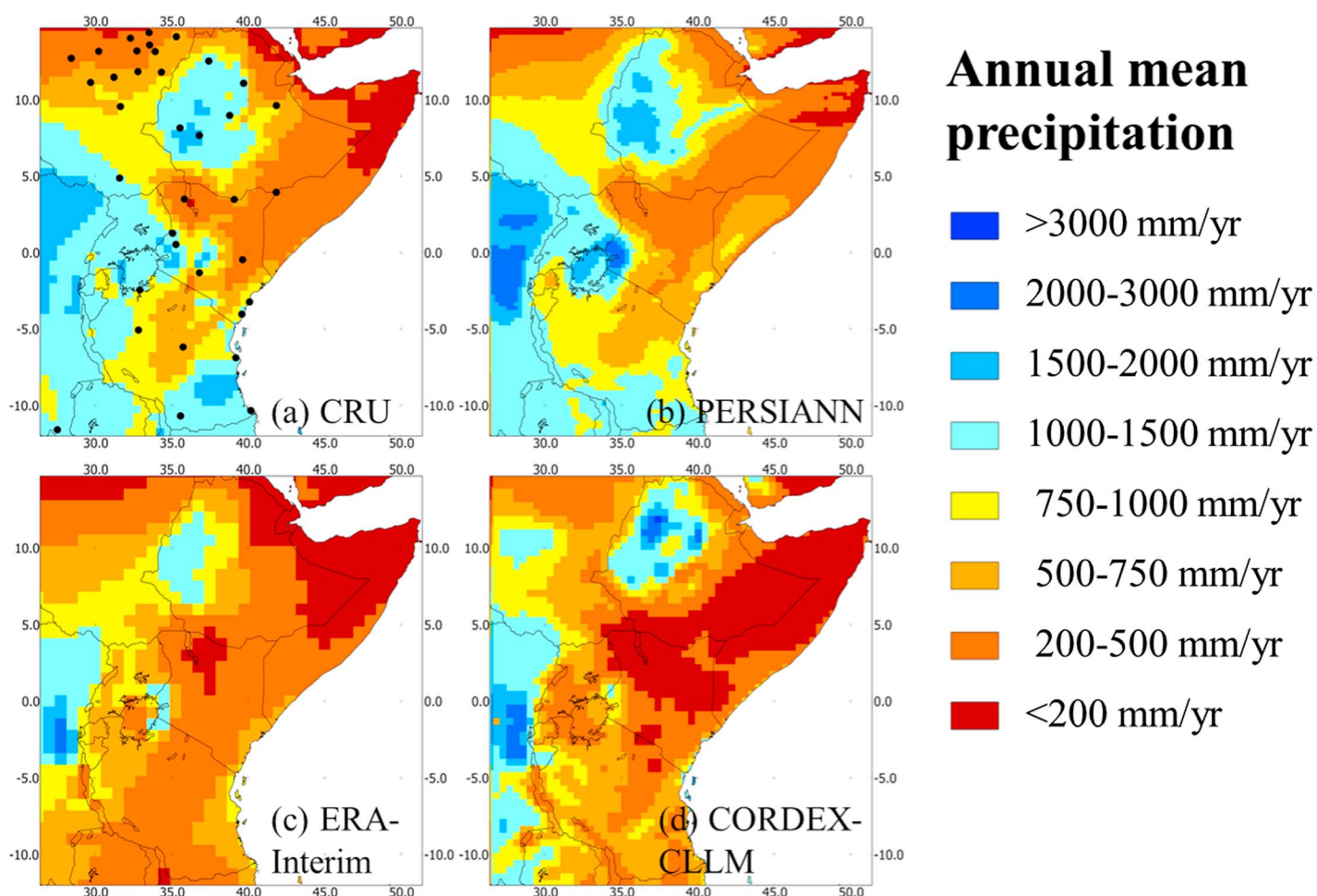
Figure 3. (a–d) Spatial distributions of mean annual precipitation for four precipitation products. The black dots in Figure 3a represent the stations that provided observational input for the CRU data set.

Such standardized, periodically published data sets often do not meet the requirements of spatiotemporal detail, operational availability, or preprocessing flexibility. A widely used alternative is the integration of historic AVHRR series with the later products [e.g., *Pedelty et al.*, 2007; *Swinnen and Veroustraete*, 2008], applying physically based empirical cross-calibration [*Gonsamo and Chen*, 2013; *Steven et al.*, 2003; *Trishchenko et al.*, 2002]. A long-term data set is generated by cross-calibration between AVHRR and SPOT-VGT. This procedure is described in detail in previous work [*Hawinkel et al.*, 2015]. It comprises resampling of LTDR v2 (0.05° resolution, 1981–1999) and SPOT-VGT (0.009° resolution, 1998–2014) to a common frame, 10 day compositing, and profile smoothing [*Eerens et al.*, 2014; *Swets et al.*, 1999]. Next, empirical cross-calibration is achieved by applying a linear VGT-to-AVHRR correction model [*Steven et al.*, 2003], estimated from corresponding, cloud-free, near-nadir pixels in the 1999 images from both data sets.

In this study, both GIMMS3g and cross-calibrated AVHRR + VGT data sets are retained for subsequent analysis over East Africa to assess the impact of temporal consistency on detected environmental effects.

3.2. Precipitation Data

Spatiotemporal studies of regional climatic effects are confronted with the scarcity and varying quality of observational data. Over Africa, precipitation records from rain gauge stations are few and spatially unevenly distributed [*Dinku et al.*, 2007]. Any interpolation approach, whether relying on pure data or employing advanced model approaches, introduces uncertainty and causes spatial and temporal heterogeneities in the quality of the end product.

Again, this has potential impacts on the conclusions about sensitivity to regional climatic variability. A review of studies on global or regional climate-vegetation interactions (see Table A1 in Appendix A) shows that most studies make use of a single data set from either one of the five following categories:

1. *Regional climate indices*: Interannual variability of a regional climate is partly driven by ocean-climate interactions across the Pacific and Indian Oceans. Various indices are derived from SSTs at predefined locations. Such indices provide a consistent and readily measurable indicator of climatic episodes at annual to decadal scales, yet without a spatial component;

2. *Rain-gauge observations*: The historical precipitation of a small region can be approximated by a limited set of rain gauge stations, with or without spatial interpolation. At larger scales, collection, quality control, and grid interpolation of available rain gauge data become a specialized workflow. Globally, the most widely used reference product is the Climate Research Unit (CRU) database (0.5° resolution, 1981–2013 [*Mitchell and Jones*, 2005]);

3. *Satellite-based/mixed rain gauge products*: Satellite sensors can measure infrared (IR) brightness and microwave (MW) reflectance, which in turn relate to precipitation intensity. Through dedicated algorithms and merging with available rain gauge observations, periodic area-covering precipitation estimates are produced. For reviews of these products over Africa, we refer to *Awange et al.* [2016], *Dinku et al.* [2007], and *Tote et al.* [2015]. Precipitation Estimation from Remotely Sensed Information using Artificial Neural Networks (PERSIANN; 0.25° resolution, 1983–2012) [*Hong et al.*, 2004; *Sorooshian et al.*, 2000] is deemed most suitable over this continent [*Awange et al.*, 2016];

4. *Model-based reanalysis products*: Extensive efforts to reconstruct the spatiotemporal distribution of climatic variables have been done through meteorological reanalysis with atmospheric models, calculating a best fit with the ensemble of available historical observations. Reanalysis products are produced by various meteorological agencies (see *Chen et al.* [1996], *Buizza et al.* [2005], *Boccara et al.* [2008], and *Duan et al.* [2012] for comparisons). One of the reference products is the ERA-Interim data set (0.75° resolution, 1979 to present [*Dee et al.*, 2011]) produced by the European Centre for Medium-Range Weather Forecasts;

5. *Climate model downscaling products*: Downscaling of atmospheric reanalysis or coarse-scale climate model outputs to higher resolution using a regional climate model (RCM) allows incorporation of a more detailed description of the particularities of that area, such as orography and lake dynamics [e.g., *Akkermans et al.*, 2014; *Docquier et al.*, 2016; *Thiery et al.*, 2015], thus providing more spatial detail than global reanalysis products.

Four spatiotemporal precipitation products were tested in parallel for their explanatory power of observed interannual vegetation patterns: (a) a gridded rain gauge interpolation product (CRU); (b) a product of merged rain gauge and satellite-based estimates (PERSIANN); (c) a reanalysis product (ERA-Interim); and (d) RCM output from the Consortium for Small-Scale Modeling model in Climate Mode (CCLM) [*Rockel et al.*, 2008], in particular a downscaling of ERA-Interim in the framework of the Coordinated Regional Climate Downscaling Experiment (CORDEX) [*Panitz et al.*, 2012]. The differences between these products are illustrated by their distributions of mean annual precipitation (Figure 3).

4. Methods

4.1. Interannual Extraction Tools

4.1.1. Ensemble Empirical Mode Decomposition (EEMD) of NDVI Time Series

Empirical mode decomposition (EMD) [*Huang et al.*, 1998] is an algorithm to iteratively extract the intrinsic time scale components from any given series. It has already been applied in studies of climate variability [*Brisson et al.*, 2015; *Coughlin and Tung*, 2005; *Molla et al.*, 2011; *Pegram et al.*, 2008] and climate effects on plant phenology [*Guan*, 2014].

Briefly, the EMD algorithm decomposes the series $X(t)$ into a set of k components isolating specific time scales with decreasing frequencies, termed intrinsic mode functions (IMF$_{i=1...k}$) and a residual term $R(t)$:

$$X(t) = \sum_i \text{IMF}_i(t) + R(t) \qquad (2)$$

Averaging ensembles of noise-added series (ensemble EMD or EEMD) [see *Wu and Huang*, 2009] yields stable IMFs representing the oscillating modes in the series. In the NDVI time series, the IMFs with estimated periods longer than 1 year are summed to reconstruct the overall interannual changes in NDVI. A detailed description of this approach and its numerical implementation are given by *Hawinkel et al.* [2015]. Interannual NDVI represents the slow modulations of the annual cycle of vegetation greenness as a smooth function over time and serves in this study as a new variable for further spatiotemporal analysis with climatic time series.
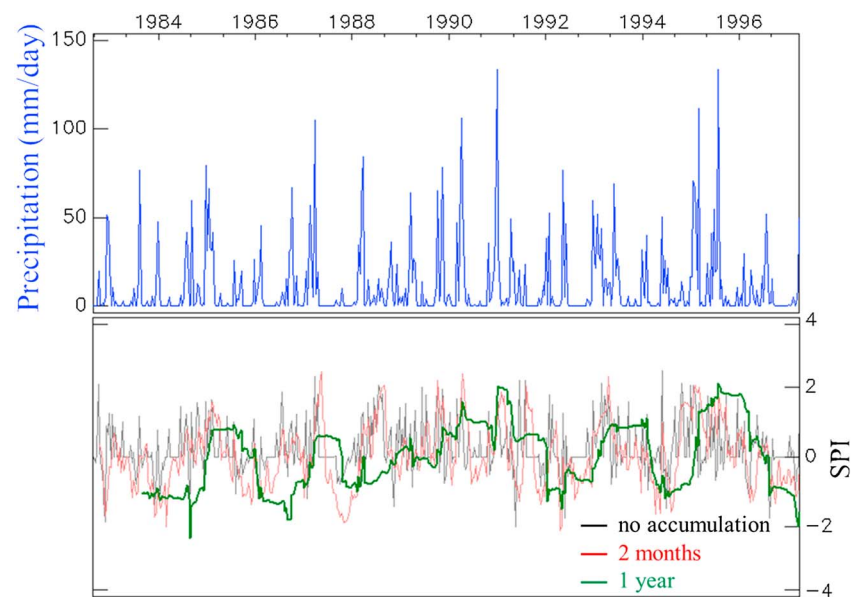
Figure 4. The standardized precipitation index (SPI) transforms precipitation events (blue) to relative scores, indicating the deviation from its expected amount for that period of the year (PERSIANN pixel in northern Kenya). SPI with 1 year accumulation time (green) provides a measure of interannual precipitation variability.

4.1.2. Standardized Precipitation Index

Precipitation occurs as discrete events over a time interval, with an underlying distribution of the probability of rainfall amounts at a certain time of the year (e.g., a 10 day period or a month, hereafter called "period"). The standardized precipitation index (SPI) [*Guttman*, 1999; *McKee et al.*, 1993] evaluates each event in a series against the estimated historic distribution for that period, taking into account the nonnormal distribution of precipitation amounts. A positive index indicates a higher than average amount of precipitation in that period.

Depending on the vegetation characteristics, soil conditions, and potential evapotranspiration rates, vegetation responds to a certain extent to the accumulated precipitation of a past time interval. Storage of water in the soil reservoir has the potential to act as a temporal buffer between precipitation events and increased soil moisture availability, with reported lag times up to 2 months [*Entin et al.*, 2000; *Koster and Suarez*, 2001; *Orth and Seneviratne*, 2012]. The effects of increased available soil moisture on the apparent greenness of vegetation display additional time lags [*Hawinkel et al.*, 2012], in particular in ecosystems with woody components [*Porporato et al.*, 2003].

A time window for accumulation of precipitation can be defined in the calculation of SPI, yielding a more smoothed indicator for longer accumulation times (Figure 4). Therefore, SPI is calculated with various accumulation periods ranging from 1 month to 2 years, in order to test the sensitivity of the detected vegetation interannual vegetation response to the size of the accumulation period for precipitation.

4.1.3. Interannual Coupling Between NDVI and Climate Variability

Interannual NDVI and accumulated SPI describe the dynamics of interannual change per pixel. The Pearson's correlation coefficient between both interannual time series quantifies the covariation of both processes and is a measure of the strength of their coupling, although without proving causation [*Lhermitte et al.*, 2011].

This quantitative measure of interannual vegetation-climate coupling per pixel is exploited in two ways. First, mapping this coupling per pixel over East Africa reveals patterns of ecological sensitivity. Alternative data products are compared with respect to the overall amount of explained response and the spatial consistency of this response to the a priori background knowledge of the study area. Second, the coupling is modeled in terms of its biogeographical explanatory factors.

4.2. Statistical Model of Interannual Coupling
4.2.1. Additive Modeling With Spatial Correlation Effects

The modeling strategy discussed here is based on the work of *Zuur et al.* [2009] and implemented in R packages *nlme* [*Pinheiro et al.*, 2015], *mgcv* [*Wood*, 2011], and *gamm4* [*Wood and Scheipl*, 2014]. Spatial

modeling of vegetation sensitivity Y in terms of biogeographical factors X_i in heterogeneous study areas is summarized in the following generic model equation:

$$Y = \alpha + \sum_i \beta_i X_i + \sum_j f_j(X_j) + \varepsilon_s \qquad (3)$$

Estimates of the linear responses β_i are obtained by minimizing the model residuals ε_s under the assumptions of ε_s being normally distributed, independent and with constant variance, allowing for hypothesis testing based on F-statistics [*Zuur et al.*, 2009]. Alternative models are compared through the Akaike information criterion (AIC) [*Akaike*, 1998], which weighs the likelihood of the estimated coefficients against the complexity of the model.

Vegetation sensitivity does not respond linearly to all controlling factors. For example, dependency on mean annual precipitation reaches a maximum in the 200–600 mm annual rainfall range [*Camberlin et al.*, 2007; *Richard and Poccard*, 1998]. For such nonlinear relationships, the linear estimator is substituted with a smoothing function $f(X_j)$ to ensure normality and equal variance of the residuals ε_s. Additive modeling [*Wood*, 2011] allows model estimation with adaptive optimization of the smoothing parameters.

The pixel-based observations and their underlying biophysical phenomena are known to be spatially correlated. The spatial covariation of residuals not accounted for by the covariates X_i and $f(X_j)$ is estimated from residual variograms and subsequently modeled in the covariance structure of ε_s using generalized additive mixed modeling (GAMM) [*Wood and Scheipl*, 2014].

All numerical variables were standardized in terms of standard deviations so that effect sizes become comparable between variables. Image data sets typically yield a very large sample size ($>$10,000) causing very weak or spurious effects to become statistically significant as measured by the F test [*Lin et al.*, 2013]. Therefore, statistical significance of effects is complemented with an evaluation of scientific significance of their effect sizes (measured by the estimated regression coefficient β_i).

4.2.2. Explanatory Biogeographical Factors

From the prior background knowledge on East Africa's climate and ecosystems, a set of biogeographic factors emerge as candidate explanatory variables to model the interannual NDVI response to precipitation variability.

Precipitation In East Africa, spanning arid ($<$250 mm yr^{-1}) to humid ($>$900 mm yr^{-1}) environments, mean annual precipitation (Figure 3) is the prime candidate driver of ecological sensitivity. Its nonlinear effect on the interannual coupling of vegetation to precipitation variability is depicted in Figure 8.

Oceanic influence The Indian Ocean Dipole Mode Index (DMI) [*Japan Agency for Marine-Earth Science and Technology (JAMSTEC)*, 2010] and the Oceanic Niño Index (ONI) [*NOAA Climate Prediction Center (NOAA-CPC)*, 2014] were selected to represent the influence of global and regional climate phenomena. Their imprint on temporal precipitation patterns gives an estimate of the spatial distributions of IOD and ENSO influence in the region. Positive phases of ENSO and IOD can cause increased precipitation amounts in multiple seasons, i.e., on the short rains [*Behera et al.*, 2005] as well as the long rains in the next year [*Indeje et al.*, 2000; *Yang et al.*, 2007]. This effect is estimated by correlating ONI and DMI series with SPI accumulated over 1 to 12 months following the ENSO or IOD phases, respectively. Also, the strength of the effect is compared between seasons by including only values per season in the calculation. An additional measure of ocean influence is each pixel's Euclidean distance to the ocean, equivalent to stream distance in *White et al.* [2005].

Topography Elevation, slope, and aspect were derived from GTOPO30 [*U.S. Geological Survey (USGS)*, 1996] at native 30 m resolution and bilinearly resampled to 20 km. Following *White et al.* [2005], topographic position and steady state wetness are characterized by the compound topographic index (CTI), obtained from the HYDRO1k geographic data set derived from GTOPO30. CTI is a function of slope and of the flow accumulation from upstream areas, and high values indicate the positions with large catchments and gentle slopes [*Moore et al.*, 1991].

Ecological zones A delineation of vegetation zones is taken from the Global Land Cover 2000 data set [*Bartholomé and Belward*, 2005]. Land cover types were reclassified and split into contiguous vegetation zones with distinct structural composition (Figure 2). Bare areas were excluded from the analysis.

Soils A map of dominant soil types is extracted from the Food and Agriculture Organization/United Nations Educational, Scientific and Cultural Organization Digital Soil Map of the World [*Food and Agriculture Organization (FAO)*, 2002].
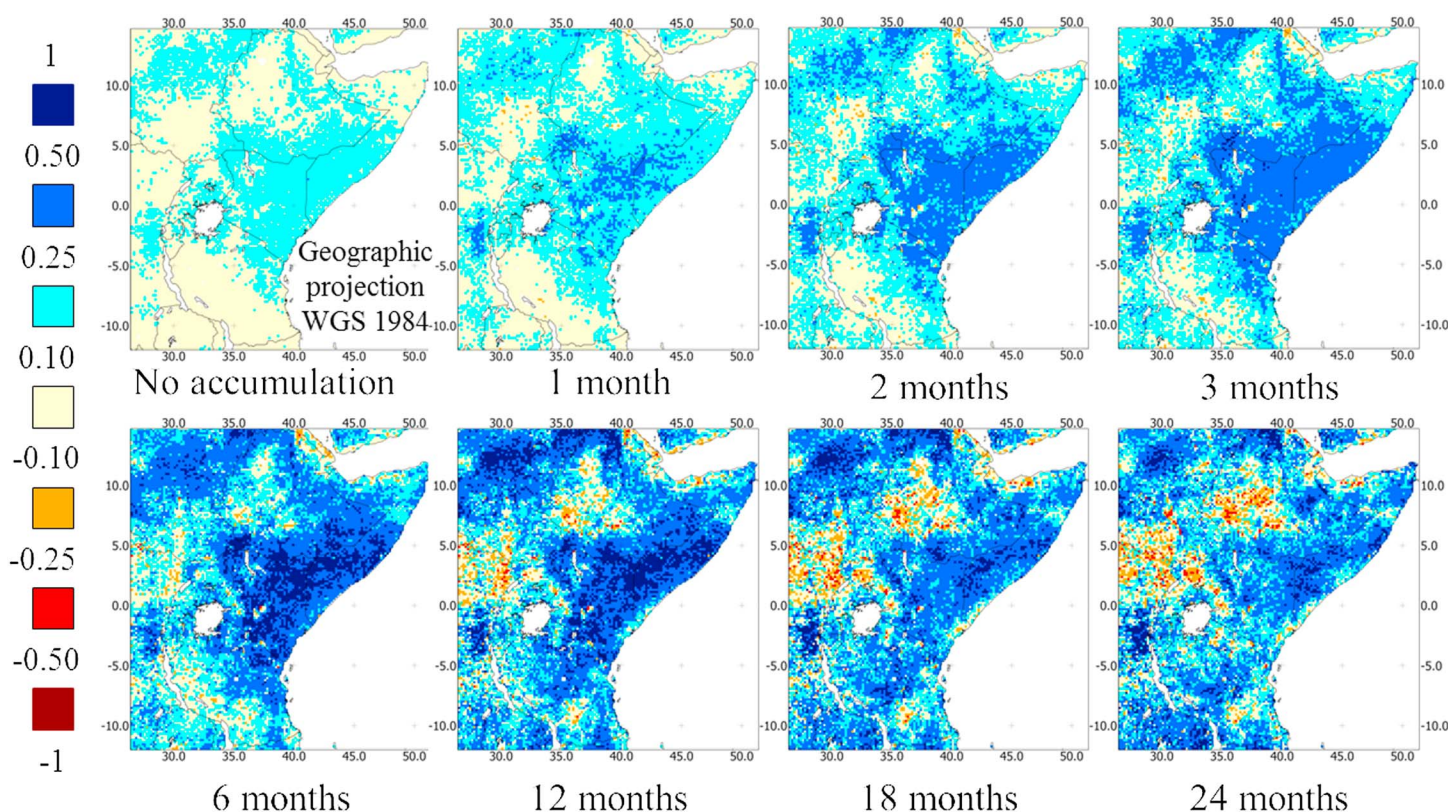
Figure 5. Correlation between precipitation (PERSIANN) and interannual NDVI time series (AVHRR + VGT) for various windows of accumulation. The explained variance levels off with precipitation accumulation over 6 to 12 months.

Interannual NDVI amplitude Finally, if the NDVI data have a low signal-to-noise ratio, then weak interannual fluctuations will not be detected accurately by EEMD [*Hawinkel et al.*, 2015]. Therefore, the amplitude of the interannual NDVI signal is added to the model to detect data-related effects.

A two-stage strategy is followed to assess the effects of the above biogeographical factors on the interannual coupling between NDVI and precipitation in East Africa. Factors linked to regional climate, oceanic influence, large-scale orography, and ecological zoning are modeled as global effects in the study area. Next, a subset of factors is modeled in more detail per ecological zone in a local effect model. The ecological zones contain 250 to 1500 pixels, making statistical hypothesis tests more effective to evaluate local effects [*Lin et al.*, 2013]. Significance at the 95% confidence interval is considered to detect meaningful effects of biogeographic factors on the interannual vegetation coupling to climate.

A detailed description of the source data and processing steps for all modeled variables can be found in the supporting information [*Bartholomé and Belward*, 2005; *Deronde et al.*, 2014; *FAO*, 2002; *Fensholt and Proud*, 2012; *Guttman*, 1999; *Hawinkel et al.*, 2015; *Hong et al.*, 2004; *JAMSTEC*, 2010; *Lhermitte et al.*, 2011; *McKee et al.*, 1993; *Mitchell and Jones*, 2005; *NASA*, 2014; *NOAA-CPC*, 2014; *Sorooshian et al.*, 2000; *USGS*, 1996; *Wu and Huang*, 2009].

5. Results

5.1. Temporal Aspects of Interannual Climate-Vegetation Coupling

The linear correlation between interannual NDVI time series extracted by EEMD and SPI is mapped per pixel over the study area for different accumulation windows of precipitation. The strength of the coupling increases when accumulation over multiple months is considered (Figure 5). However, accumulation over more than 12 months does not add to the explained variance. Interannual NDVI response to 1 year accumulated SPI is further used as the indicator for vegetation response to climate variability.
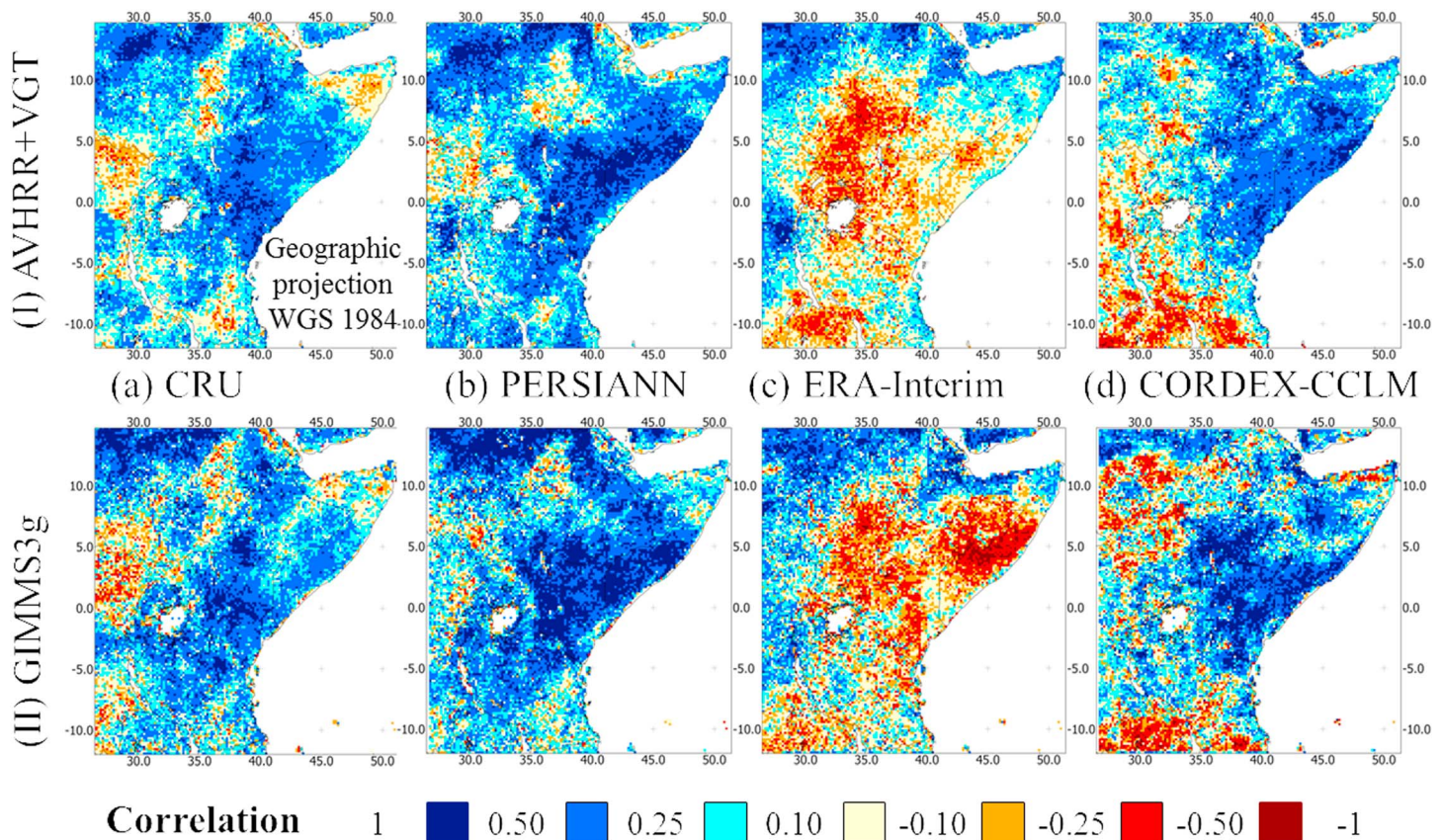
Figure 6. (a–d) Detected coupling between interannual NDVI (AVHRR + VGT and GIMMS3g) and 1 year accumulated SPI using four different data products. Overall explained variability and the occurrence of zonal anomalies are relative measures to compare quality across data products.

5.2. Spatial Patterns of Interannual Climate-Vegetation Coupling

The precipitation products can be ranked with respect to overall explained response and spatial consistency with the patterns described in section 2 (Figure 6). ERA-Interim displays highly different couplings, inconsistent with other products and with expected patterns of strong coupling in lowland areas exposed to the Indian Ocean. The CORDEX-CCLM model output yields more subtle deviations from the other products, but strong zonal anomalies indicate lower spatial consistency, particularly in the most southern latitude band of the study area. For the two observational products, i.e., CRU and PERSIANN, the patterns of precipitation sensitivity conform to the a priori expected patterns with reduced coupling to rainfall in mountainous regions as well as in both extremely dry and humid zones. Discrepancies in detections between AVHRR + VGT and GIMMS3g are local and not significant enough to reject either of both data sets at this stage.

5.3. Controlling Biogeographical Factors
5.3.1. Influence of ENSO and IOD Phenomena in East Africa

The imprint of ENSO on SPI series is strongest when considering precipitation in the 6 months following the ENSO phase. For IOD, the effect on precipitation was detected most strongly 4 months after each IOD phase. Also, the season in which the effects on precipitation anomalies are most pronounced differs for both indices (Figure 7). The short rains are heavily driven by IOD, while the effect of ENSO is slightly weaker but extends into the period of long rains.

5.3.2. Global Effects

A generalized additive mixed model (GAMM) with a smooth term for mean annual precipitation, global biogeographic factors, and spatially correlated residuals is applied to all combinations of AVHRR + VGT and GIMMS3g and PERSIANN and CRU, respectively. The full model results, relative effect sizes per factors, and their statistical significance are presented in Table A2 in Appendix A. The models explain 28% to 43% of
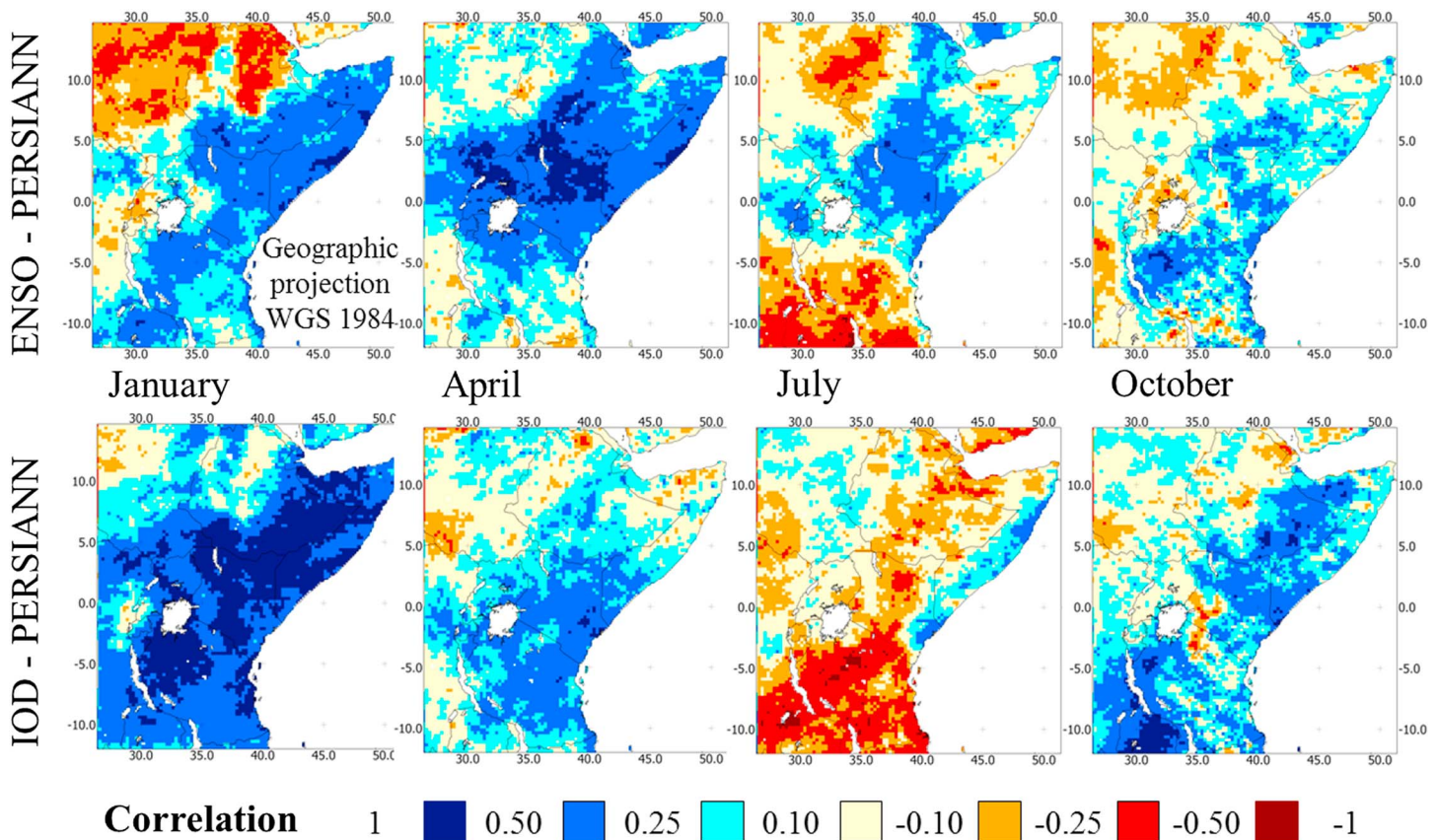
Figure 7. The influence of (top) ENSO (ONI index) and (bottom) IOD (DMI index) on precipitation anomalies measured by SPI differs per season. ENSO phases have effects up to 6 months later in the long rainy season, while IOD has strong effects on the short rains up to 4 months after each positive phase.

the observed variability in vegetation response. Measured by AIC, inclusion of spatially correlated residuals is the strongest determining factor for the model's performance.

For all data set combinations, the models agree on the significant effects of mean annual precipitation, vegetation type, and elevation. The nonlinear effect of mean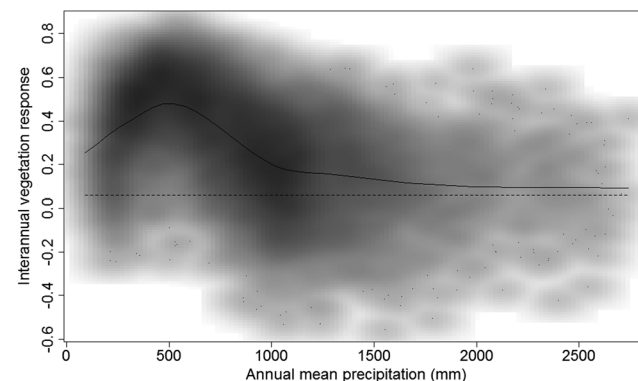 annual precipitation on the interannual NDVI response to precipitation is depicted in Figure 8. ENSO and IOD forcing of precipitation is not reflected in interannual NDVI patterns in the global model for the study area. These effects are further examined per ecological zone in a local effects model (section 5.3.3). Soil type and CTI are not found to influence the interannual NDVI response to precipitation variability.

The global effect model residuals for the GIMMS3g/PERSIANN data sets are depicted in Figure 9, along with the observed coupling and the predictions from the additive model. The residuals display spatial correlation with an estimated range of 250–300 km in all directions (Figure 9c). Large negative residuals (overestimations of the response) occur (i) in sparsely vegetated areas in

Figure 8. The nonlinear relationship between the interannual vegetation response (AVHRR + VGT) to precipitation variability (PERSIANN) and annual mean precipitation over East Africa (1981–2014). Maximum sensitivity occurs in semiarid and subhumid areas with mean annual precipitation around 500 mm. Additive models account for nonlinear effects on the response variable with smoothing terms (black line). The dashed line indicates the 95% confidence level for the per-pixel correlation between time series (sample size = 726 time steps).
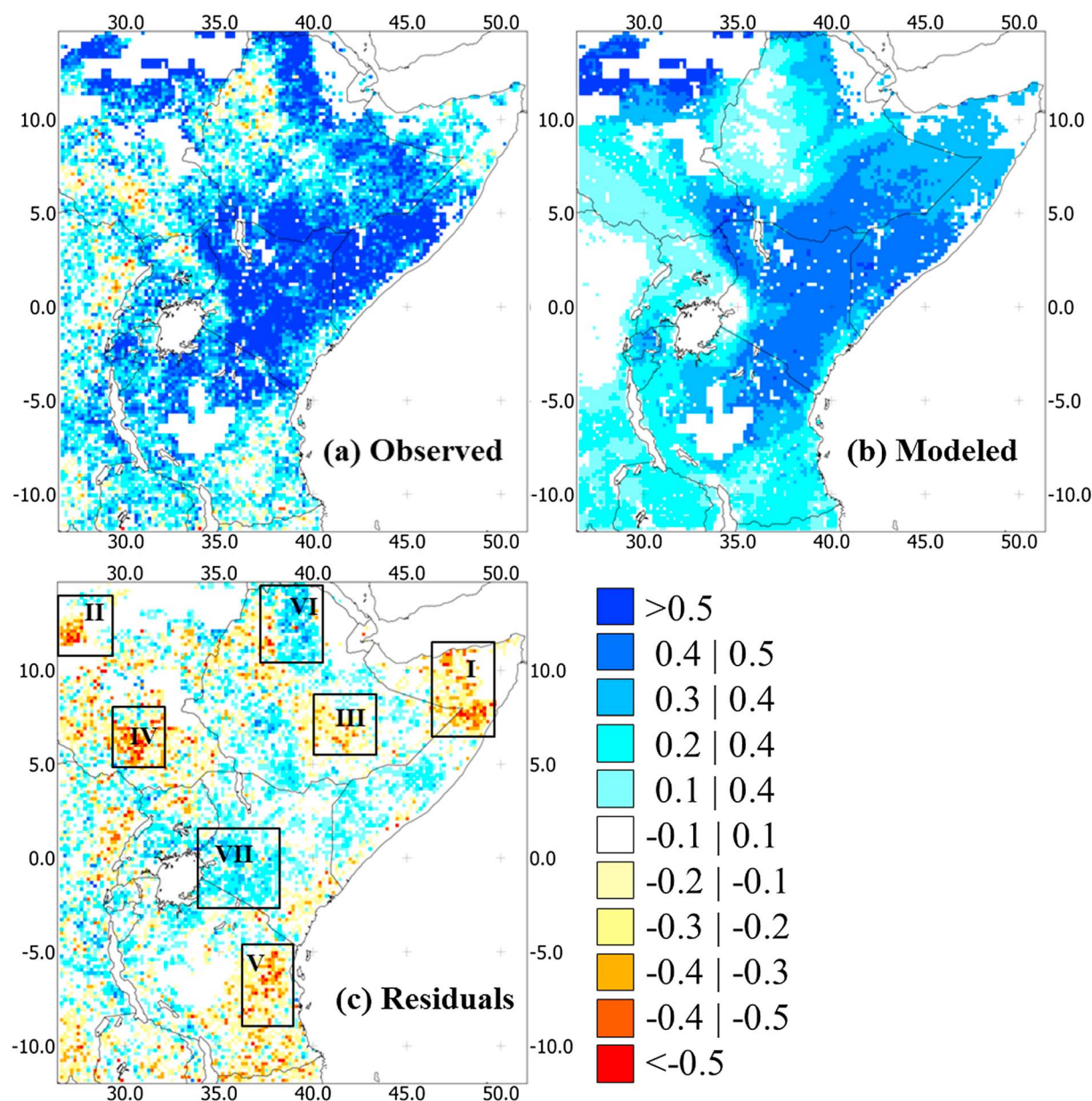
Figure 9. (a) The observed coupling of interannual NDVI (GIMMS3g) to precipitation variability (PERSIANN). (b) The model predictions from global effects across the study area. (c) The spatial distribution of residuals, with Roman numerals highlighting the clusters of large residuals.

the Horn of Africa; (ii) in the eastern end of the Sahel region, which belongs to a system dominated by the West African monsoon [*Nicholson*, 2013] and falls de facto largely outside the study area; (iii) in the eastern Ethiopian Highlands; (iv) in a part of the shrublands of South Sudan; and (v) in the tropical woodlands and savannahs in the southeastern part of the study area. The response is underestimated for (vi) the cropland regions of northern Ethiopia and (vii) for the extremely wet area east of Lake Victoria (large positive residuals). The latter may be caused by either an overestimation of precipitation by PERSIANN (Figure 3b) or by a biased estimation of the nonlinear relationship to mean annual precipitation in the data-scarce upper tail of the distribution (Figure 8). Elsewhere, residuals are moderate in size and distributed near randomly.

Model disagreement between data set combinations highlights the impact of spatiotemporal inconsistency in data products. The choice of precipitation product mainly affects the detected effect of distance to the Indian Ocean. This relatively coarse measure captures any systematic effects related to data quality along the
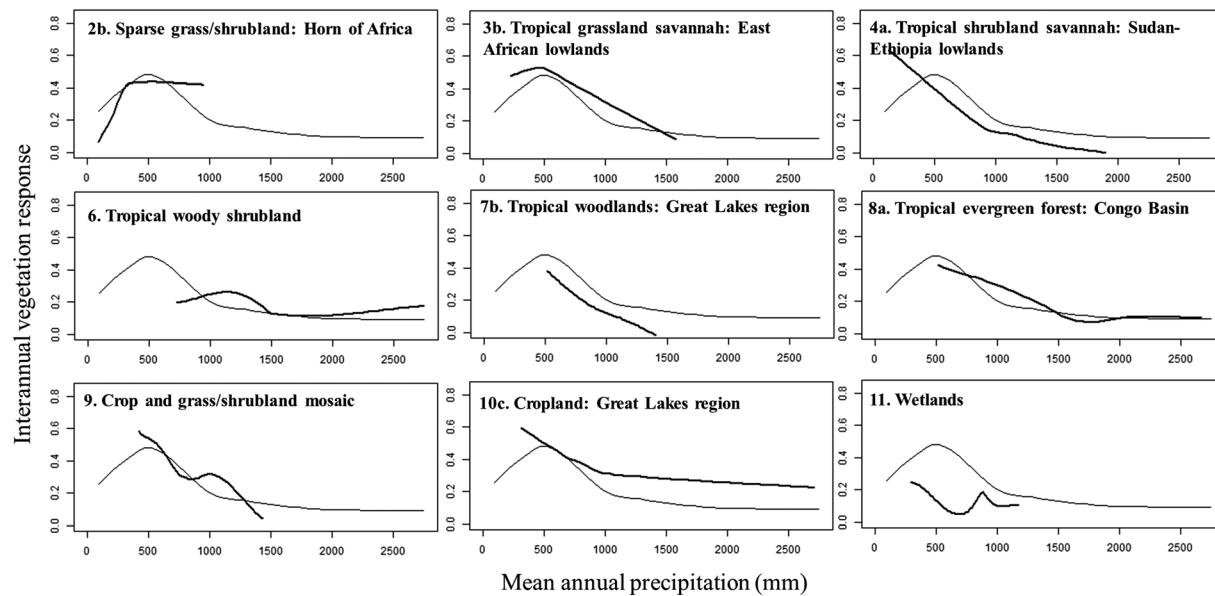
Figure 10. The effect of mean annual precipitation on the interannual vegetation response to climate variability varies per ecological zone. The local response (bold line) deviates from the overall curve for East Africa (thin line).

longitudinal gradient. As can be seen from Figure 3a, station coverage for the CRU data set is very low in the western part of the study area, where remarkably lower coupling is detected with CRU as compared with PERSIANN (Figures 3a and 3b). For interannual NDVI detected from the AVHRR + VGT data set, response to precipitation variability decreases sharply with elevation, whereas this effect is only moderate when detected with GIMMS3g. For highland areas exceeding 1200 m, a systematically lower response is detected from AVHRR + VGT.

5.3.3. Local Effects

The nonlinear effect of mean annual precipitation is estimated within each ecological zone in order to examine its deviation from the global curve for East Africa (Figure 10). These local deviations include overall higher sensitivity in cropland areas (plot 10c) and grassland savannah (plot 3b), lower sensitivity in tropical woodlands (plot 4a), and a shift in maximum sensitivity toward higher precipitation ($1200 \, \mathrm{mm \, yr^{-1}}$) for tropical woody shrublands (plot 6). Only in the sparse grassland and shrubland in the Horn of Africa, sensitivity to precipitation variability does not decrease in the parts receiving relatively more precipitation annually, stressing this region's vulnerability. In wetlands and regularly flooded areas (plot 11), interannual vegetation response is decoupled from variability in precipitation amounts.

The local effects of ENSO and IOD influence as well as local topography effects are tabulated in Table A3 in Appendix A. The influence of IOD and ENSO on the coupling of vegetation and precipitation dynamics in East African ecosystems appear to have a spatial as well as an ecological limit. IOD influence (notably on the short rains) explains a portion of the interannual vegetation response to precipitation variability in the subhumid ecosystems of the African Great Lakes region receiving 500–900 mm of precipitation annually. These include savannah systems with shrub and woody components, woody shrublands, and the associated cropland systems. Effects of ENSO in the subsequent long rainy season do not show further impacts on the interannual vegetation response, only weakly in the lowland savannah along the Indian Ocean, and northwest of the East African Rift valley where precipitation anomalies are out of phase with the ENSO modes (Figure 7). Elevation has a negative effect on the interannual vegetation response to precipitation only in the cropland systems on the Ethiopian plateau, where temperature limitations start to be significant.

6. Discussion

6.1. Impacts of Data Uncertainty

Parallel analyses of multiple data products highlight the importance of uncertainty in spatiotemporal data sets in long-term ecological studies. This is particularly the case for precipitation products over data-scarce regions

such as East Africa. It is hypothesized that satellite-based products will display the most homogeneous quality over station-scarce regions [*Moazami et al.*, 2014; *Pfeifroth et al.*, 2012], for they do not rely on wide interpolations or underlying atmospheric and topography models. Whereas rain gauge networks and MW sensors provide data with a clear physical link to precipitation amounts, they suffer from sparse spatial coverage and poor temporal sampling, respectively. Near-polar orbiting IR sensors provide complementary spatial and temporal detail, although with no direct physical link to precipitation [*Yong et al.*, 2012]. Merging procedures [see, e.g., *Huffman et al.*, 1995] balance accuracy with spatiotemporal coverage and are therefore deemed superior for use in regional long-term spatiotemporal studies.

The results indicate against the use of reanalysis products (ERA-Interim) over areas where data assimilation is limited and strong orography challenges coarse-resolution atmospheric models. Their lower performance in terms of precipitation representation in the East African Great Lakes region relative to CORDEX-CCLM was confirmed earlier by *Thiery et al.* [2015, 2016]. The difference between results from station-based CRU and satellite-based PERSIANN is remarkably low, prompting an upward revision of the quality of CRU with respect to the initial hypothesis.

Temporal inconsistency in the NDVI time series due to, among others, imperfect sensor intercalibration and orbital drift effects was also found to impact detection of environmental effects, although of smaller impact than spatial inconsistency in precipitation products. Particularly at higher elevations (>1200 m), detected responses are negatively affected by residual artifacts in the AVHRR + VGT series. This may be attributable to an either lower performance of cloud detection over mountainous areas in the LTDR of SPOT-VGT processing chains or to orbital drift effects of the VGT2 sensor [*Swinnen et al.*, 2014], causing changing illumination conditions with possibly stronger effects over rugged terrain. For dense vegetation with near 100% canopy cover, the NDVI displays saturation effects in its upper range [*Asner et al.*, 2003; *Sellers*, 1985], which weakens the relationship to biomass productivity [*Gu et al.*, 2013; *Mutanga and Skidmore*, 2004]. This adds uncertainty to the estimation of annual and interannual vegetation responses of tropical forests [*Huete et al.*, 2006] as well as in dense canopy cropland [*Thenkabail et al.*, 2000]. More advanced spectral indices can reduce the saturation effect [*Huete et al.*, 2002; *Jiang et al.*, 2008] but are not consistently available for historical analysis extending 30 years back in time.

6.2. Detection of Interannual Variability

EEMD as interannual extraction tool [*Hawinkel et al.*, 2015] is able to highlight the total interannual component in NDVI time series, regardless of the nature or variable timing of annual growing season across the study area. This flexibility improves upon earlier approaches with either the assumption of an invariable annual season per zone [*Camberlin et al.*, 2007; *De Keersmaecker et al.*, 2015; *Plisnier et al.*, 2000] or the filtering of predefined multiannual time scales imposed by harmonic or wavelet methods [e.g., *Immerzeel et al.*, 2005; *Martínez and Gilabert*, 2009]. Interannual NDVI by EEMD thus provides a new key variable for detecting climate-driven changes in vegetation greenness over large areas without prior assumptions on its time scales.

Interannual variability of precipitation can be captured by SPI by converting series of discrete rainfall events into smoothed, normalized anomalies. However, particular care must be taken when defining the accumulation period. Soil memory effects in the atmosphere-land moisture cycle [*Orth and Seneviratne*, 2012] may explain only part of the observed delay between precipitation anomalies and greenness response (Figure 5). Moreover, this effect is limited by the soil's water-holding capacity, which is strongly related to the density of the vegetation cover [*Koster and Suarez*, 2001]. An explanation for the fact that precipitation anomalies over a 6 to 12 month window impact vegetation greenness can therefore not be purely hydrological. *Holmgren et al.* [2013] found that precipitation anomalies in semiarid ecosystems trigger changes in tree cover by increased tree recruitment and alteration of fire regimes. Such nonlinear pathways surpass the capability of modeling precipitation-vegetation interactions at a subcontinental scale but can be approximated by considering linear correlations with delay and accumulation effects over multiple seasons.

It must be noted as well that deriving interannual NDVI and SPI from their initial physical quantities (red and infrared surface reflectance and precipitation amounts, respectively) inevitably lowers their signal-to-noise ratio: the EEMD algorithm removes the dominant annual mode and introduces a large amount of temporal interpolation, whereas the stochastic and measurement noise present in precipitation series propagates in accumulated SPI calculations. Their relationship may not be linear, particularly along the very humid portion

of the precipitation gradient ($>2000 \, \text{mm} \, \text{yr}^{-1}$) [*Guan et al.*, 2015]. As a result, detected correlations are moderate in magnitude and must be interpreted relative to the population of pixels rather than as absolute values per pixel. If the absolute strength of the interannual vegetation response to precipitation variability for a particular set of locations would be at interest, a nonlinear measure of coupling such as Spearman's rank correlation could further improve accuracy.

6.3. Biogeographical Controls on Ecosystem Sensitivity

On the scale of East Africa, the interannual response of vegetation greenness to precipitation variability is determined most strongly by the structural characteristics and of the vegetation itself, rather than through climatic-oceanic influence or topographic factors. Ecosystems dominated by herbaceous cover (sparse grass and shrublands, grassland savannahs, and croplands) display the largest overall response to anomalous precipitation (Figure 9a). In this vegetation zone, even the relatively humid areas receiving 1000 mm of precipitation annually display persistent higher sensitivity (Figure 10, plots 2b, 3b, and 10c). These semiarid and subhumid areas, characterized by pastoral grazing and mixed cereal cropping systems, are likely to suffer severe production losses in case of extended drought episodes [*Adhikari et al.*, 2015; *Barron et al.*, 2003; *Schlenker and Lobell*, 2010; *Thornton et al.*, 2009] with implicit risks for food security [*Brown and Funk*, 2008; *Lobell et al.*, 2008]. In the presence of woody components, the modifying role of mean annual precipitation on the interannual vegetation response approaches the average regional curve (Figure 8), with a decreasing sensitivity beyond 500 mm of annual precipitation. In the transition zone between tropical evergreen forest and woody savannah, a shifted peak in sensitivity toward 1200 mm/year is observed (Figure 10, plot 6). This has severe implications for the stability of the rainforests in the Democratic Republic of Congo at their northern edge, where forest degradation due to reduced precipitation and subsequent alteration of the canopy structure has been confirmed by remote sensing observations and climatological data [*Asefi-Najafabady and Saatchi*, 2013; *Zhou et al.*, 2014].

The influence of coupled oceanic-atmospheric phenomena is mostly reflected in precipitation variability rather than in interannual vegetation response. Our findings on the timing of IOD forcing on precipitation (Figure 7) confirm that IOD phases cause anomalous precipitation during the short rains [*Behera et al.*, 2005; *Black et al.*, 2003], while the effect ENSO episodes are observed also the subsequent long rains [*Indeje et al.*, 2000]. Both phenomena are known to have strong linkages [*Behera et al.*, 2005; *Black et al.*, 2003], but their precise interaction is still being investigated [*Williams and Hanan*, 2011].

Although the influence of IOD and ENSO on the interannual coupling between vegetation and precipitation variability is of less significance than the role of mean annual precipitation and vegetation type, its spatial and ecological limits provide new insights in the region's vulnerability to climate variability. The subhumid ecosystems of the African Great Lakes region ($500–900 \, \text{mm} \, \text{yr}^{-1}$) are most strongly coupled to climatic fluctuations caused by IOD and ENSO. This subregion encompasses densely populated areas with mixed cropland and agroforestry systems associated with woody shrublands and of savannah systems with shrub and woody components. The overall lower sensitivity to precipitation variability compared to the treeless ecosystems mentioned above is thus not guaranteed in case of persistent multiannual climate anomalies spelled by IOD or ENSO. *Hirota et al.* [2011] have identified critical transitions on tree cover when ecosystem-dependent tipping points are crossed, an aspect which has not been accounted for in present-day climate models. Near-real time monitoring of IOD and ENSO teleconnections is therefore essential in developing early warning systems for drought risk in East Africa [*Pozzi et al.*, 2013; *Pulwarty and Sivakumar*, 2014]. *Ivory et al.* [2013] found that the impact of interannual climatic variability on vegetation is also expressed through fluctuations in atmospheric circulation resulting in alterations of the dry season length. SST-derived indices such as ONI and DMI are thus not the sole indicators of imminent wet and dry episodes.

Despite the strong role of East Africa's topography in shaping its climate systems [*Anyah et al.*, 2006; *Indeje et al.*, 2001], the direct effects of local topography on ecosystem sensitivity are minor compared to the overall effects of vegetation type and mean annual precipitation. *White et al.* [2005] found a larger role of elevation and slope in temperate regions, where temperature and solar energy influx are more limiting.

7. Conclusions

Regional assessments of vegetation response to climate variability inevitably rely on spatiotemporal data sets with inherent quality limitations. From a wide range of observation and interpolation strategies, satellite-based

Table A1. Review of Climate Data Sets Used in Studies on the Spatiotemporal Response of Vegetation to Climate Variability[a]

Data Set	Studies
(a) Climate indices (no spatial component)	
ENSO index from sea surface temperature (SST) anomalies [*Ropelewski and Halpert*, 1986; *Trenberth*, 1997; *Trenberth and Stepaniak*, 2001; *Woodruff et al.*, 1987]	*Anyamba and Eastman* [1996], *Myneni et al.* [1996], *Plisnier et al.* [2000], *Mennis* [2001], *Nicholson et al.* [2001], and *White et al.* [2005]
Southern Niño Oscillation Index (SOI) [*Ropelewski and Jones*, 1987]	*Li and Kafatos* [2000], *Plisnier et al.* [2000], and *Prasad et al.* [2007]
Multivariate ENSO Index (MEI) [*Wolter and Timlin*, 1998, 2011]	*Brown et al.* [2010], *Propastin et al.* [2010], and *van Leeuwen et al.* [2013]
Indian Ocean Dipole/Dipole Mode Index (IOD/DMI) [*Saji et al.*, 1999]	*Prasad et al.* [2007] and *Brown et al.* [2010]
Pacific Decadal Oscillation (PDO) [*Mantua et al.*, 1997]	*Brown et al.* [2010]
(b) Station rain gauge observations (with or without grid interpolation)	
Climate Research Unit (CRU) database [*Mitchell and Jones*, 2005, *New et al.*, 2000] grid interpolations	*Camberlin et al.* [2007], *Hirota et al.* [2011], *Holmgren et al.* [2001], *De Jong et al.* [2013], and *Ibrahim et al.* [2015]
Global Precipitation Climatology Center (GPCC) [*Becker et al.*, 2013] grid interpolations	*Nezlin et al.* [2005]
VASClimO product [*Beck et al.*, 2004] grid interpolations	*Bai et al.* [2008]
Standardized Precipitation and Evapotranspiration Index (SPEI), based on updated CRU-gridded data product [*Harris et al.*, 2014]	*Ivits et al.* [2014] and *De Keersmaecker et al.* [2015]
Regional station observations (with custom spatial interpolation)	*Richard and Poccard* [1998], *Kawabata et al.* [2001], *Omuto et al.* [2010], and *Guo et al.* [2014]
Regional station observations (without interpolation)	*Nicholson and Farrar* [1994], *Plisnier et al.* [2000], *Nicholson et al.* [2001], *Li et al.* [2002], *Prasad et al.* [2007], *Wessels et al.* [2007], *Zhou et al.* [2009], and *Brando et al.* [2010]
(c) Satellite-based estimates and mixed rain gauge satellite products	
Tropical Rainfall Measuring Mission (TRMM) [*Kummerow et al.*, 2000]	*Herrmann et al.* [2005] and *Hilker et al.* [2014]
Tropical Applications of Meteorology using Satelite data and ground observations (TAMSAT) [*Grimes et al.*, 1999]	*Brandt et al.* [2015]
Global Precipitation Climatology Project (GPCP) version 2 monthly precipitation analysis [*Adler et al.*, 2003]	*Herrmann et al.* [2005]
NOAA Climate Prediction Center (CPC) Rainfall Estimator version 2.0 (RFE2.0) [*Herman et al.*, 1997; *Xie and Arkin*, 1996]	*Kileshye Onema and Taigbenu* [2009]
NOAA Climate Prediction Center (CPC) Merged Analysis of Precipitation (CMAP) [*Xie and Arkin*, 1997]	*Camberlin et al.* [2007]
Precipitation Estimation from Remotely Sensed Information using Artificial Neural Networks (PERSIANN) [*Hong et al.*, 2004; *Sorooshian et al.*, 2000]	*Clinton et al.* [2014]
(d) Model-based data assimilation and reanalysis products	
European Centre for Medium-Range Weather Forecasts (ECMWF) ERA-40 Reanalysis	*Swinnen* [2008]
Global Land Data Assimilation System (GLDAS) [*Rodell et al.*, 2004]	*Myoung et al.* [2013]
Natural Resources Canada daily data [*Hutchinson et al.*, 2009; *McKenney et al.*, 2011]	*Li et al.* [2013]
(e) Regional climate model downscaling outputs	
ECHAM4 [*Roeckner et al.*, 1996]–Regional Model (REMO) [*Jacob et al.*, 2001]	*Schmidt et al.* [2014]
ECHAM5 [*Roeckner et al.*, 2003]–COSMO-CLM^2 [*Davin et al.*, 2011]	*Akkermans et al.* [2014]

[a]Five categories can be distinguished, ranging from pure data-based to more model-based products.

Table A2. Global Effects of Biogeographical Factors on the Interannual Vegetation Response to Climate Variability are Estimated Using Different Combinations of Input Data[a]

	AVHRR + VGT/PERSIANN		AVHRR + VGT/CRU		GIMMS/PERSIANN		GIMMS/CRU	
Mean precipitation	smooth	***	smooth	***	smooth	***	smooth	***
Interannual NDVI amplitude	0.11	***	0.03	***	0.06	***	0.05	***
IOD influence	−0.03	.	−0.01		0.04	.	0.01	
ENSO influence	−0.01		0.00		0.00		0.01	
Elevation	−0.17	***	−0.14	***	−0.05	**	−0.04	**
CTI	−0.01	*	0.00		0.00		0.00	
Distance to ocean	−0.03		−0.16	***	0.01		−0.22	***
Ecological zone		***		***		**		***
Soil type				*				
Model-adjusted R^2	0.43		0.31		0.36		0.28	
$P(X > |F|)$ in F test: $0 <$ *** < 0.001** < 0.01* $< 0.05 < . < 0.1$							$N = 11,361$	

[a]Relative effect sizes are shown for parametric terms, along with indications of their statistical significance.

estimates deliver the most homogeneous quality over areas with scarce direct ground observations. Nevertheless, we recommend to evaluate any ecological hypothesis in a setup with multiple alternative data products and to critically test detected outcomes against the potential effect of data-related bias.

Environmental effect models combine the flexibility to model multiple linear and nonlinear ecological effects with statistical robustness for large spatially correlated samples, for example, via generalized additive mixed models (GAMMs). Models must be adapted to the scale of the effects (regional to local) and be evaluated iteratively to infer meaningful conclusions on biogeographical factors determining the vegetation response.

In the water-limited ecosystems of East Africa, mean annual precipitation explains the bulk of variability in vegetation response across ecological zones. More locally, topographic and soil factors play a limited role. The influence of coupled ocean-atmosphere phenomena affects vegetation response within limits defined by orography and ecological zones. Overall, ecosystems with dominant herbaceous components are most sensitive to interannual precipitation variability. However, also woody shrubland and woodland systems are affected by prolonged climate anomalies that occur with IOD and ENSO phases. The applied assessment strategy is transferable to other regions, with due attention for data quality evaluation and review of region-specific links with the global climate. Proper identification of ecological strata and identification of meaningful biogeographical factors is critical in constructing models to describe complex spatiotemporal vegetation response for the evaluation of climate change sensitivity.

Appendix A: Climate Data Sets Used in Spatiotemporal Studies on Vegetation Response

Table A3. Local Effects of ENSO, IOD, and Topography on the Interannual Vegetation Response (GIMMS3g) to Precipitation Variability (PERSIANN)[a]

Ecological Zones (Figure 2)	3b. Tropical Grassland Savannah: East African Lowlands		4b. Tropical Shrubland Savannah: Great Lakes		5a. Tropical Woody Savannah: Sudan Lowlands		5b. Tropical Woody Savannah: Great Lakes		6. Tropical Woody Shrubland		9. Crop and Grass/ Shrubland Mosaic		10b. Cropland: Ethiopian Plateau		10c. Cropland: Great Lakes	
ENSO influence	−0.07	*	−0.07		0.14	*	−0.07		0.09		−0.17	***	0.04		−0.09	
IOD influence	0.01		0.16	*	0.24		0.17	*	0.18	*	−0.37	*	−0.07		0.25	***
Elevation	0.01		0.12		−0.05		−0.01		−0.02		−0.21		−0.16	*	−0.01	
Sample size (N)	2217		712		357		991		534		441		1027		849	
$P(X > |F|)$ in F test: $0 <$ *** < 0.001** < 0.01* $< 0.05 < . < 0.1$																

[a]Relative effect sizes are tabulated along with their statistical significance.

References

Adhikari, U., A. P. Nejadhashemi, and S. A. Woznicki (2015), Climate change and eastern Africa: A review of impact on major crops, *Food Energy Secur.*, *4*, 110–132.

Adler, R. F., et al. (2003), The version-2 Global Precipitation Climatology Project (GPCP) monthly precipitation analysis (1979–present), *J. Hydrometeorol.*, *4*, 1147–1167.

Akaike, H. (1998), Information theory and an extension of the maximum likelihood principle, in *Selected Papers of Hirotugu Akaike: Springer Series in Statistics*, edited by E. Parzen, K. Tanabe, and G. Kitagawa, pp. 199–213, Springer, New York.

Akkermans, T., W. Thiery, and N. P. M. Van Lipzig (2014), The regional climate impact of a realistic future deforestation scenario in the Congo Basin, *J. Clim.*, *27*, 2714–2734.

Anyah, R. O., and F. H. M. Semazzi (2006), Climate variability over the Greater Horn of Africa based on NCAR AGCM ensemble, *Theor. Appl. Climatol.*, *86*, 39–62.

Anyah, R. O., and F. H. M. Semazzi (2007), Variability of East African rainfall based on multiyear RegCM3 simulations, *Int. J. Climatol.*, *27*, 357–371.

Anyah, R. O., F. H. M. Semazzi, and L. Xie (2006), Simulated physical mechanisms associated with climate variability over Lake Victoria basin in East Africa, *Mon. Weather Rev.*, *134*, 3588–3609.

Anyamba, A., and J. R. Eastman (1996), Interannual variability of NDVI over Africa and its relation to El Niño–Southern Oscillation, *Int. J. Remote Sens.*, *17*, 2533–2548.

Asefi-Najafabady, S., and S. Saatchi (2013), Response of African humid tropical forests to recent rainfall anomalies, *Philos. Trans. R. Soc. B: Biol. Sci.*, *368*, 20120306, doi:10.1098/rstb.2012.0306.

Asner, G. P., J. M. O. Scurlock, and J. A. Hicke (2003), Global synthesis of leaf area index observations: Implications for ecological and remote sensing studies, *Global Ecol. Biogeogr.*, *12*, 191–205.

Awange, J. L., V. G. Ferreira, E. Forootan, S. Khandu, A. Andam-Akorful, N. O. Agutu, and X. F. He (2016), Uncertainties in remotely sensed precipitation data over Africa, *Int. J. Climatol.*, *36*, 303–323.

Ba, M. B., and S. E. Nicholson (1998), Analysis of convective activity and its relationship to the rainfall over the Rift Valley lakes of East Africa during 1983–90 using the Meteosat infrared channel, *J. Appl. Meteorol.*, *37*, 1250–1264.

Bai, Z. G., D. L. Dent, L. Olsson, and M. E. Schaepman (2008), Proxy global assessment of land degradation, *Soil Use Manage.*, *24*, 223–234.

Barron, J., J. Rockstrom, F. Gichuki, and N. Hatibu (2003), Dry spell analysis and maize yields for two semi-arid locations in east Africa, *Agric. For. Meteorol.*, *117*, 23–37.

Bartholomé, E., and A. S. Belward (2005), GLC2000: A new approach to global land cover mapping from Earth observation data, *Int. J. Remote Sens.*, *26*, 1959–1977.

Beck, C., J. Grieser, and B. Rudolf (2004), *A New Monthly Precipitation Climatology for the Global Land Areas for the Period 1951 to 2000*, *Clim. Status Rep.*, German Weather Serv, Offenbach, Germany.

Becker, A., P. Finger, A. Meyer-Christoffer, B. Rudolf, K. Schamm, U. Schneider, and M. Ziese (2013), A description of the global land-surface precipitation data products of the Global Precipitation Climatology Centre with sample applications including centennial (trend) analysis from 1901–present, *Earth Syst. Sci. Data*, *5*, 71–99.

Behera, S. K., J.-J. Luo, S. Masson, P. Delecluse, S. Gualdi, A. Navarra, and T. Yamagata (2005), Paramount impact of the Indian Ocean Dipole on the East African short rains: A CGCM study, *J. Clim.*, *18*, 4514–4530.

Black, E., J. Slingo, and K. R. Sperber (2003), An observational study of the relationship between excessively strong short rains in coastal East Africa and Indian Ocean SST, *Mon. Weather Rev.*, *131*, 74–94.

Boccara, G., A. Hertzog, C. Basdevant, and F. Vial (2008), Accuracy of NCEP/NCAR reanalyses and ECMWF analyses in the lower stratosphere over Antarctica in 2005, *J. Geophys. Res.*, *113*, D20115, doi:10.1029/2008JD010116.

Brando, P. M., S. J. Goetz, A. Baccini, D. C. Nepstad, P. S. A. Beck, and M. C. Christman (2010), Seasonal and interannual variability of climate and vegetation indices across the Amazon, *Proc. Natl. Acad. Sci. U.S.A.*, *107*, 14,685–14,690.

Brandt, M., C. Mbow, A. A. Diouf, A. Verger, C. Samimi, and R. Fensholt (2015), Ground-and satellite-based evidence of the biophysical mechanisms behind the greening Sahel, *Global Change Biol.*, *21*, 1610–1620.

Braswell, B. H., D. S. Schimel, E. Linder, and B. Moore (1997), The response of global terrestrial ecosystems to interannual temperature variability, *Science*, *278*, 870–873.

Brisson, E., M. Demuzere, P. Willems, and N. M. van Lipzig (2015), Assessment of natural climate variability using a weather generator, *Clim. Dyn.*, *44*, 495–508.

Brown, M. E., K. de Beurs, and A. Vrieling (2010), The response of African land surface phenology to large scale climate oscillations, *Remote Sens. Environ.*, *114*, 2286–2296.

Brown, M. E., and C. C. Funk (2008), Climate—Food security under climate change, *Science*, *319*, 580–581.

Buizza, R., P. L. Houtekamer, G. Pellerin, Z. Toth, Y. Zhu, and M. Wei (2005), A comparison of the ECMWF, MSC, and NCEP global ensemble prediction systems, *Mon. Weather Rev.*, *133*, 1076–1097.

Busby, J. W., T. G. Smith, and N. Krishnan (2014), Climate security vulnerability in Africa mapping 3.01, *Political Geogr.*, *43*, 51–67.

Camberlin, P., N. Martiny, N. Philippon, and Y. Richard (2007), Determinants of the interannual relationships between remote sensed photosynthetic activity and rainfall in tropical Africa, *Remote Sens. Environ.*, *106*, 199–216.

Chen, F., K. Mitchell, J. Schaake, Y. Xue, H.-L. Pan, V. Koren, Q. Y. Duan, M. Ek, and A. Betts (1996), Modeling of land surface evaporation by four schemes and comparison with FIFE observations, *J. Geophys. Res.*, *101*, 7251–7268, doi:10.1029/95JD02165.

Clinton, N., L. Yu, H. Fu, C. He, and P. Gong (2014), Global-scale associations of vegetation phenology with rainfall and temperature at a high spatio-temporal resolution, *Remote Sens.*, *6*, 7320–7338.

Conway, D., C. E. Hanson, R. Doherty, and A. Persechino (2007), GCM simulations of the Indian Ocean Dipole influence on East African rainfall: Present and future, *Geophys. Res. Lett.*, *34*, L03705, doi:10.1029/2006GL027597.

Cooper, P. J. M., J. Dimes, K. P. C. Rao, B. Shapiro, B. Shiferaw, and S. Twomlow (2008), Coping better with current climatic variability in the rain-fed farming systems of sub-Saharan Africa: An essential first step in adapting to future climate change?: Agriculture, *Ecosyst. Environ.*, *126*, 24–35.

Coughlin, K., and K. K. Tung (2005), Empirical mode decomposition of climate variabilty in the atmosphere, in *Hilbert-Huang Transform and Its Applications*, edited by N. Huang and S. Shen, pp. 149–166, World Scientific, Singapore.

Cracknell, A. P. (2001), The exciting and totally unanticipated success of the AVHRR in applications for which it was never intended, *Adv. Space Res.*, *28*, 233–240.

Dardel, C., L. Kergoat, P. Hiernaux, E. Mougin, M. Grippa, and C. J. Tucker (2014), Re-greening Sahel: 30 years of remote sensing data and field observations (Mali, Niger), *Remote Sens. Environ.*, *140*, 350–364.

Davin, E., R. Stöckli, E. Jaeger, S. Levis, and S. Seneviratne (2011), COSMO-CLM2: A new version of the COSMO-CLM model coupled to the Community Land Model, *Clim. Dyn.*, *37*, 1889–1907.

De Jong, R., M. E. Schaepman, R. Furrer, S. De Bruin, and P. H. Verburg (2013), Spatial relationship between climatologies and changes in global vegetation activity, *Global Change Biol.*, *19*, 1953–1964.

De Keersmaecker, W., S. Lhermitte, L. Tits, O. Honnay, B. Somers, and P. Coppin (2015), A model quantifying global vegetation resistance and resilience to short-term climate anomalies and their relationship with vegetation cover, *Global Ecol. Biogeogr.*, *24*, 539–548.

Dee, D. P., et al. (2011), The ERA-Interim reanalysis: Configuration and performance of the data assimilation system, *Q. J. R. Meteorol. Soc.*, *37*, 553–597.

Deronde, B., W. Debruyn, E. Gontier, E. Goor, T. Jacobs, S. Verbeiren, and J. Vereecken (2014), 15 years of processing and dissemination of SPOT-VEGETATION products, *Int. J. Remote Sens.*, *35*, 2402–2420.

Dierckx, W., S. Sterckx, I. Benhadj, S. Livens, G. Duhoux, T. Van Achteren, M. Francois, K. Mellab, and G. Saint (2014), PROBA-V mission for global vegetation monitoring: Standard products and image quality, *Int. J. Remote Sens.*, *35*, 2589–2614.

Dinku, T., P. Ceccato, E. Grover-Kopec, M. Lemma, S. J. Connor, and C. F. Ropelewski (2007), Validation of satellite rainfall products over East Africa's complex topography, *Int. J. Remote Sens.*, *28*, 1503–1526.

Docquier, D., W. Thiery, S. Lhermitte, and N. Lipzig (2016), Multi-year wind dynamics around Lake Tanganyika, *Clim. Dyn.*, 1–12, doi:10.1007/s00382-016-3020-z.

Duan, M., J. Ma, and P. Wang (2012), Preliminary comparison of the CMA, ECMWF, NCEP, and JMA ensemble prediction systems, *Acta Meteorol. Sin.*, *26*, 26–40.

Dubovyk, O., G. Menz, and A. Khamzina (2012), Trend analysis of MODIS time-series using different vegetation indices for monitoring of cropland degradation and abandonment in central Asia, in *IEEE International Geoscience and Remote Sensing Symposium (IGARSS) 2012*, pp. 6589–6592, IEEE Press, Munich, Germany.

Eerens, H., D. Haesen, F. Rembold, F. Urbano, C. Tote, and L. Bydekerke (2014), Image time series processing for agriculture monitoring, *Environ. Modell. Software*, *53*, 154–162.

Entin, J. K., A. Robock, K. Y. Vinnikov, S. E. Hollinger, S. Liu, and A. Namkhai (2000), Temporal and spatial scales of observed soil moisture variations in the extratropics, *J. Geophys. Res.*, *105*, 11,865–11,877, doi:10.1029/2000JD900051.

FAO (2002), *FAO/UNESCO Digital Soil Map of the World and Derived Soil Properties*, FAO, Rome.

Farrar, T. J., S. E. Nicholson, and A. R. Lare (1994), The influence of soil type on the relationships between NDVI, rainfall, and soil moisture in semiarid Botswana. II. NDVI response to soil moisture, *Remote Sens. Environ.*, *50*, 121–133.

Fensholt, R., and S. R. Proud (2012), Evaluation of Earth observation based global long term vegetation trends—Comparing GIMMS and MODIS global NDVI time series, *Remote Sens. Environ.*, *119*, 131–147.

Fensholt, R., K. Rasmussen, P. Kaspersen, S. Huber, S. Horion, and E. Swinnen (2013), Assessing land degradation/recovery in the African Sahel from long-term Earth observation based primary productivity and precipitation relationships, *Remote Sens.*, *5*, 664–686.

Giannini, A., M. Biasutti, I. Held, and A. Sobel (2008), A global perspective on African climate, *Clim. Change*, *90*, 359–383.

Gonsamo, A., and J. M. Chen (2013), Spectral response function comparability among 21 satellite sensors for vegetation monitoring, *IEEE Trans. Geosci. Remote Sens.*, *51*, 1319–1335.

Greve, M., A. M. Lykke, A. Blach-Overgaard, and J.-C. Svenning (2011), Environmental and anthropogenic determinants of vegetation distribution across Africa, *Global Ecol. Biogeogr.*, *20*, 661–674.

Grimes, D. I. F., E. Pardo-Igúzquiza, and R. Bonifacio (1999), Optimal areal rainfall estimation using raingauges and satellite data, *J. Hydrol.*, *222*, 93–108.

Gu, Y., B. K. Wylie, D. M. Howard, K. P. Phuyal, and L. Ji (2013), NDVI saturation adjustment: A new approach for improving cropland performance estimates in the Greater Platte River Basin, USA, *Ecol. Indic.*, *30*, 1–6.

Guan, B. T. (2014), Ensemble empirical mode decomposition for analyzing phenological responses to warming, *Agric. For. Meteorol.*, *194*, 1–7.

Guan, K., et al. (2015), Photosynthetic seasonality of global tropical forests constrained by hydroclimate, *Nat. Geosci.*, *8*, 284–289.

Guillod, B. P., B. Orlowsky, D. G. Miralles, A. J. Teuling, and S. I. Seneviratne (2015), Reconciling spatial and temporal soil moisture effects on afternoon rainfall, *Nat. Commun.*, *6*, 6443, doi:10.1038/ncomms7443.

Guo, W., X. Ni, D. Jing, and S. Li (2014), Spatial-temporal patterns of vegetation dynamics and their relationships to climate variations in Qinghai Lake Basin using MODIS time-series data, *J. Geogr. Sci.*, *24*, 1009–1021.

Guttman, N. B. (1999), Accepting the standardized precipitation index: A calculation algorithm, *J. Am. Water Resour. Assoc.*, *35*, 311–322.

Harris, I., P. D. Jones, T. J. Osborn, and D. H. Lister (2014), Updated high-resolution grids of monthly climatic observations—The CRU TS3.10 dataset, *Int. J. Climatol.*, *34*, 623–642.

Hawinkel, P., E. Swinnen, S. Lhermitte, B. Verbist, J. Van Orshoven, and B. Muys (2015), A time series processing tool to extract climate-driven interannual vegetation dynamics using ensemble empirical mode decomposition (EEMD), *Remote Sens. Environ.*, *169*, 375–389.

Hawinkel, P., E. Swinnen, C. Tote, and J. Van Orshoven 2012, Assessing vegetation response to climate variability via time series of NDVI, precipitation and soil moisture content, 1st EARSeL Workshop on Temporal Analysis of Satellite Images, 23rd–25th May, 2012, Mykonos, Greece.

Herman, A., V. B. Kumar, P. A. Arkin, and J. V. Kousky (1997), Objectively determined 10-day African rainfall estimates created for famine early warning systems, *Int. J. Remote Sens.*, *18*, 2147–2159.

Herrmann, S. M., A. Anyamba, and C. J. Tucker (2005), Recent trends in vegetation dynamics in the African Sahel and their relationship to climate, *Global Environ. Change*, *15*, 394–404.

Hilker, T., A. I. Lyapustin, C. J. Tucker, F. G. Hall, R. B. Myneni, Y. J. Wang, J. Bi, Y. M. de Moura, and P. J. Sellers (2014), Vegetation dynamics and rainfall sensitivity of the Amazon, *Proc. Natl. Acad. Sci. U.S.A.*, *111*, 16,041–16,046.

Hirabayashi, Y., R. Mahendran, S. Koirala, L. Konoshima, D. Yamazaki, S. Watanabe, H. Kim, and S. Kanae (2013), Global flood risk under climate change, *Nature Clim. Change*, *3*, 816–821.

Hirota, M., M. Holmgren, E. H. Van Nes, and M. Scheffer (2011), Global resilience of tropical forest and savanna to critical transitions, *Science*, *334*, 232–235.

Holmgren, M., M. Scheffer, E. Ezcurra, J. Gutiérrez, and G. F. J. Mohren (2001), El Niño effects on the dynamics of terrestrial ecosystems, *Trends Ecol. Evol.*, *16*, 89–94.

Holmgren, M., M. Hirota, E. H. van Nes, and M. Scheffer (2013), Effects of interannual climate variability on tropical tree cover, *Nat. Clim. Change*, *3*, 755–758.

Hong, Y., K.-L. Hsu, S. Sorooshian, and X. Gao (2004), Precipitation estimation from remotely sensed imagery using an artificial neural network cloud classification system, *J. Appl. Meteorol.*, *43*, 1834–1853.

Huang, N. E., Z. Shen, S. R. Long, M. C. Wu, H. H. Shih, Q. Zheng, N.-C. Yen, C. C. Tung, and H. H. Liu (1998), The empirical mode decomposition and the Hilbert spectrum for nonlinear and non-stationary time series analysis, *Proc. R. Soc. London*, *454*, 903–995.

Huete, A., K. Didan, T. Miura, E. P. Rodriguez, X. Gao, and L. G. Ferreira (2002), Overview of the radiometric and biophysical performance of the MODIS vegetation indices, *Remote Sens. Environ.*, *83*, 195–213.

Huete, A. R., K. Didan, Y. E. Shimabukuro, P. Ratana, S. R. Saleska, L. R. Hutyra, W. Yang, R. R. Nemani, and R. Myneni (2006), Amazon rainforests green-up with sunlight in dry season, *Geophys. Res. Lett.*, *33*, L06405, doi:10.1029/2005GL025583.

Huffman, G. J., R. F. Adler, B. Rudolf, U. Schneider, and P. R. Keehn (1995), Global precipitation estimates based on a technique for combining satellite-based estimates, rain gauge analysis, and NWP model precipitation information, *J. Clim.*, *8*, 1284–1295.

Hutchinson, M. F., D. W. McKenney, K. Lawrence, J. H. Pedlar, R. F. Hopkinson, E. Milewska, and P. Papadopol (2009), Development and testing of Canada-wide interpolated spatial models of daily minimum–maximum temperature and precipitation for 1961–2003, *J. Appl. Meteorol. Climatol.*, *48*, 725–741.

Ibrahim, Y. Z., H. Balzter, J. Kaduk, and C. J. Tucker (2015), Land degradation assessment using residual trend analysis of GIMMS NDVI3g, soil moisture and rainfall in sub-Saharan West Africa from 1982 to 2012, *Remote Sens.*, *7*, 5471–5494.

Immerzeel, W. W., R. A. Quiroz, and S. M. De Jong (2005), Understanding precipitation patterns and land use interaction in Tibet using harmonic analysis of SPOT VGT-S10 NDVI time series, *Int. J. Remote Sens.*, *26*, 2281–2296.

Indeje, M., F. H. M. Semazzi, and L. J. Ogallo (2000), ENSO signals in East African rainfall seasons, *Int. J. Climatol.*, *20*, 19–46.

Indeje, M., F. H. M. Semazzi, L. Xie, and L. J. Ogallo (2001), Mechanistic model simulations of the East African climate using NCAR Regional Climate Model: Influence of large-scale orography on the Turkana low-level jet, *J. Clim.*, *14*, 2710–2724.

IPCC (2014), *Climate Change 2014: Impacts, Adaptation, and Vulnerability. Part A: Global and Sectoral Aspects. Contribution of Working Group II to the Fifth Assessment Report of the Intergovernmental Panel on Climate Change*, edited by C. B. Field et al., 1132 pp., Cambridge University Press, Cambridge, U. K., and New York.

Ivits, E., S. Horion, R. Fensholt, and M. Cherlet (2014), Drought footprint on European ecosystems between 1999 and 2010 assessed by remotely sensed vegetation phenology and productivity, *Global Change Biol.*, *20*, 581–593.

Ivory, S. J., J. Russell, and A. S. Cohen (2013), In the hot seat: Insolation, ENSO, and vegetation in the African tropics, *J. Geophys. Res. Biogeosciences*, *118*, 1347–1358, doi:10.1002/jgrg.20115.

Jacob, D., et al. (2001), A comprehensive model inter-comparison study investigating the water budget during the BALTEX-PIDCAP period, *Meteorol. Atmos. Phys.*, *77*, 19–43.

JAMSTEC (2010), *Indian Ocean Dipole Mode Index (DMI). Japan Agency for Marine-Earth Science and Technology*, Yokosuka, Japan.

Jiang, Z., A. R. Huete, K. Didan, and T. Miura (2008), Development of a two-band enhanced vegetation index without a blue band, *Remote Sens. Environ.*, *112*, 3833–3845.

Jönsson, P., and L. Eklundh (2002), Seasonality extraction by function fitting to time-series of satellite sensor data, *IEEE Trans. Geosci. Remote Sens.*, *40*, 1824–1832.

Kawabata, A., K. Ichii, and Y. Yamaguchi (2001), Global monitoring of interannual changes in vegetation activities using NDVI and its relationships to temperature and precipitation, *Int. J. Remote Sens.*, *22*, 1377–1382.

Kileshye Onema, J.-M., and A. Taigbenu (2009), NDVI–rainfall relationship in the Semliki watershed of the equatorial Nile, *Phys. Chem. Earth, Parts A/B/C*, *34*, 711–721.

Kizza, M., A. Rodhe, C.-Y. Xu, H. Ntale, and S. Halldin (2009), Temporal rainfall variability in the Lake Victoria Basin in East Africa during the twentieth century, *Theor. Appl. Climatol.*, *98*, 119–135.

Knox, J., T. Hess, A. Daccache, and T. Wheeler (2012), Climate change impacts on crop productivity in Africa and South Asia, *Environ. Res. Lett.*, *7*, 8.

Koster, R. D., and M. J. Suarez (2001), Soil moisture memory in climate models, *J. Hydrometeorol.*, *2*, 558–570.

Kummerow, C., et al. (2000), The status of the Tropical Rainfall Measuring Mission (TRMM) after two years in orbit, *J. Appl. Meteorol.*, *39*, 1965–1982.

Laing, A. G., R. E. Carbone, and V. Levizzani (2011), Cycles and propagation of deep convection over equatorial Africa, *Mon. Weather Rev.*, *139*, 2832–2853.

Lanckriet, S., A. Frankl, E. Adgo, P. Termonia, and J. Nyssen (2015), Droughts related to quasi-global oscillations: A diagnostic teleconnection analysis in North Ethiopia, *Int. J. Climatol.*, *35*, 1534–1542.

Lauwaet, D. (2009), The influence of land use changes on precipitation in the Sahel, Ph.D. thesis, KU Leuven, Leuven, 149 p.

Lhermitte, S., J. Verbesselt, I. Jonckheere, K. Nackaerts, J. A. N. van Aardt, W. W. Verstraeten, and P. Coppin (2008), Hierarchical image segmentation based on similarity of NDVI time series, *Remote Sens. Environ.*, *112*, 506–521.

Lhermitte, S., J. Verbesselt, W. W. Verstraeten, and P. Coppin (2011), A comparison of time series similarity measures for classification and change detection of ecosystem dynamics, *Remote Sens. Environ.*, *115*, 3129–3152.

Li, B., S. Tao, and R. W. Dawson (2002), Relations between AVHRR NDVI and ecoclimatic parameters in China, *Int. J. Remote Sens.*, *23*, 989–999.

Li, Z., T. Huffman, B. McConkey, and L. Townley-Smith (2013), Monitoring and modeling spatial and temporal patterns of grassland dynamics using time-series MODIS NDVI with climate and stocking data, *Remote Sens. Environ.*, *138*, 232–244.

Li, Z., and Z. Kafatos (2000), Interannual variability of vegetation in the United States and its relation to El Niño/Southern Oscillation, *Remote Sens. Environ.*, *71*, 239–247.

Lillesø, J.-P. B., et al. 2011, Potential natural vegetation of eastern Africa. Volume 1: The Atlas, Forest & Landscape Working Paper 61-2011, World Agroforestry Centre.

Lin, M., H. C. Lucas, and G. Shmueli (2013), Research commentary—Too big to fail: Large samples and the *p*-value problem, *Information Syst. Res.*, *24*, 906–917.

Liu, M., H. Tian, G. Chen, W. Ren, C. Zhang, and J. Liu (2008), Effects of land-use and land-cover change on evapotranspiration and water yield in China during 1900-2001, *J. Am. Water Resour. Assoc.*, *44*, 1193–1207.

Lobell, D. B., M. B. Burke, C. Tebaldi, M. D. Mastrandrea, W. P. Falcon, and R. L. Naylor (2008), Prioritizing climate change adaptation needs for food security in 2030, *Science*, *319*, 607–610.

Luo, Y., et al. (2011), Coordinated approaches to quantify long-term ecosystem dynamics in response to global change, *Global Change Biol.*, *17*, 843–854.

Luyssaert, S., et al. (2007), CO_2 balance of boreal, temperate, and tropical forests derived from a global database, *Global Change Biol.*, *13*, 2509–2537.

Maidment, R. I., D. I. F. Grimes, R. P. Allan, H. Greatrex, O. Rojas, and O. Leo (2013), Evaluation of satellite-based and model re-analysis rainfall estimates for Uganda, *Meteorol. Appl.*, *20*, 308–317.

Mantua, N. J., S. R. Hare, Y. Zhang, J. M. Wallace, and R. C. Francis (1997), A Pacific interdecadal climate oscillation with impacts on salmon production, *Bull. Am. Meteorol. Soc.*, *78*, 1069–1079.

Marchant, R., C. Mumbi, S. Behera, and T. Yamagata (2007), The Indian Ocean Dipole—The unsung driver of climatic variability in East Africa, *Afr. J. Ecol.*, *45*, 4–16.

Martínez, B., and M. A. Gilabert (2009), Vegetation dynamics from NDVI time series analysis using the wavelet transform, *Remote Sens. Environ.*, *113*, 1823–1842.

McKee, T. B., N. J. Doesken, and J. Kliest, 1993, The relationship of drought frequency and duration to time scales, Proceedings of the 8th Conference of Applied Climatology, 17-22 January, p. 179-184.

McKenney, D. W., M. F. Hutchinson, P. Papadopol, K. Lawrence, J. Pedlar, K. Campbell, E. Milewska, R. F. Hopkinson, D. Price, and T. Owen (2011), Customized spatial climate models for North America, *Bull. Am. Meteorol. Soc.*, *92*, 1611–1622.

Mennis, J. (2001), Exploring relationships between ENSO and vegetation vigour in the south-east USA using AVHRR data, *Int. J. Remote Sens.*, *22*, 3077–3092.

Mitchell, T. D., and P. D. Jones (2005), An improved method of constructing a database of monthly climate observations and associated high-resolution grids, *Int. J. Climatol.*, *25*, 693–712.

Moazami, S., S. Golian, Y. Hong, C. Sheng, and M. R. Kavianpour (2014), Comprehensive evaluation of four high-resolution satellite precipitation products over diverse climate conditions in Iran, *Hydrol. Sci. J.*, doi:10.1080/02626667.2014.987675.

Molla, M. K. I., P. R. Ghosh, and K. Hirose (2011), Bivariate EMD-based data adaptive approach to the analysis of climate variability, *Discrete Dyn. Nat. Soc.*, *2011*, 21.

Moore, I. D., R. B. Grayson, and A. R. Ladson (1991), Digital terrain modelling: A review of hydrological, geomorphological, and biological applications, *Hydrol. Process.*, *5*, 3–30.

Mutanga, O., and A. K. Skidmore (2004), Narrow band vegetation indices overcome the saturation problem in biomass estimation, *Int. J. Remote Sens.*, *25*, 3999–4014.

Myneni, R. B., S. O. Los, and C. J. Tucker (1996), Satellite-based identification of linked vegetation index and sea surface temperature anomaly areas from 1982-1990 for Africa, Australia and South America, *Geophys. Res. Lett.*, *23*, 729–732, doi:10.1029/96GL00266.

Myoung, B., Y.-S. Choi, S. Hong, and S. K. Park (2013), Inter- and intra-annual variability of vegetation in the northern hemisphere and its association with precursor meteorological factors, *Global Biogeochem. Cycles*, *27*, 31–42, doi:10.1002/gbc.20017.

Nagol, J. R., E. F. Vermote, and S. D. Prince (2014), Quantification of impact of orbital drift on inter-annual trends in AVHRR NDVI data, *Remote Sens.*, *6*, 6680–6687.

NASA (2014), Land long term data record. [Available at http://ltdr.nascom.nasa.gov/cgi-bin/ltdr/ltdrPage.cgi?fileName=LTDR_update], last accessed 24 June 2015., National Aeronautics and Space Administration, Washington, D. C.

New, M., M. Hulme, and P. Jones (2000), Representing twentieth-century space–time climate variability. Part II: Development of 1901–96 monthly grids of terrestrial surface climate, *J. Clim.*, *13*, 2217–2238.

Nezlin, N. P., A. G. Kostianoy, and B.-L. Li (2005), Inter-annual variability and interaction of remote-sensed vegetation index and atmospheric precipitation in the Aral Sea region, *J. Arid Environ.*, *62*, 677–700.

Nicholson, S. E. (2013), The West African Sahel: A review of recent studies on the rainfall regime and its interannual variability, *ISRN Meteorol.*, *2013*, 1–32.

Nicholson, S. E., M. Davenport, and A. Malo (1990), A comparison of the vegetation response to rainfall in the Sahel and East Africa, using normalized difference vegetation index from NOAA AVHRR, *Clim. Change*, *17*, 209–241.

Nicholson, S. E., and T. J. Farrar (1994), The influence of soil type on the relationships between NDVI, rainfall, and soil moisture in semiarid Botswana. I. NDVI response to rainfall, *Remote Sens. Environ.*, *50*, 107–120.

Nicholson, S. E., D. Leposo, and J. Grist (2001), The relationship between El Niño and drought over Botswana, *J. Clim.*, *14*, 323–335.

NOAA-CPC (2014), Historic El Niño/La Niña episodes (1950-present). [Available at http://www.cpc.noaa.gov/products/analysis_monitoring/ensostuff/ensoyears.shtml], last accessed 24 June 2015., Climate Prediction Center, National Oceanic and Atmospheric Administration.

Omondi, P., L. A. Ogallo, R. Anyah, J. M. Muthama, and J. Ininda (2013), Linkages between global sea surface temperatures and decadal rainfall variability over eastern Africa region, *Int. J. Climatol.*, *33*, 2082–2104.

Omuto, C. T., R. R. Vargas, M. S. Alim, and P. Paron (2010), Mixed-effects modelling of time series NDVI-rainfall relationship for detecting human-induced loss of vegetation cover in drylands, *J. Arid Environ.*, *74*, 1552–1563.

Orth, R., and S. I. Seneviratne (2012), Analysis of soil moisture memory from observations in Europe, *J. Geophys. Res.*, *117*, D15115, doi:10.1029/2011JD017366.

Panitz, H.-J., P. Berg, G. Schädler, and G. Fosser (2012), Modelling near future regional climate change for Germany and Africa, in *High Performance Computing in Science and Engineering '11*, edited by W. E. Nagel, D. B. Kröner, and M. M. Resch, pp. 503–512, Springer, Berlin, Heidelberg.

Pedelty, J., et al. (2007), Generating a long-term land data record from the AVHRR and MODIS instruments, in *IEEE International Geoscience and Remote Sensing Symposium (IGARSS)*, pp. 1021–1025, IEEE, Barcelona, Spain.

Pegram, G. G. S., M. C. Peel, and T. A. McMahon (2008), Empirical mode decomposition using rational splines: An application to rainfall time series, *Proc. R. Soc. A*, *464*, 1483–1501.

Pettorelli, N., J. O. Vik, A. Mysterud, J.-M. Gaillard, C. J. Tucker, and N. C. Stenseth (2005), Using the satellite-derived NDVI to assess ecological responses to environmental change, *Trends Ecol. Evol.*, *20*, 503–510.

Pfeifroth, U., R. Mueller, and B. Ahrens (2012), Evaluation of satellite-based and reanalysis precipitation data in the tropical Pacific, *J. Appl. Meteorol. Climatol.*, *52*, 634–644.

Philippon, N., P. Camberlin, V. Moron, and J. Boyard-Micheau (2015), Anomalously wet and dry rainy seasons in equatorial East Africa and associated differences in intra-seasonal characteristics, *Clim. Dyn.*, *45*, 1819–1840.

Piao, S. L., X. H. Wang, P. Ciais, B. Zhu, T. Wang, and J. Liu (2011), Changes in satellite-derived vegetation growth trend in temperate and boreal Eurasia from 1982 to 2006, *Global Change Biol.*, *17*, 3228–3239.

Pinheiro, J., D. Bates, S. DebRoy, D. Sarkar, and R. Core Team (2015), nlme: Linear and nonlinear mixed effects models, R package version 3.1-120.

Plisnier, P. D., S. Serneels, and E. F. Lambin (2000), Impact of ENSO on East African ecosystems: A multivariate analysis based on climate and remote sensing data, *Global Ecol. Biogeogr.*, *9*, 481–497.

Porporato, A., F. Laio, L. Ridolfi, K. K. Caylor, and I. Rodriguez-Iturbe (2003), Soil moisture and plant stress dynamics along the Kalahari precipitation gradient, *J. Geophys. Res.*, *108*(D3), 4127, doi:10.1029/2002JD002448.

Pozzi, W., et al. (2013), Toward global drought early warning capability: Expanding international cooperation for the development of a framework for monitoring and forecasting, *Bull. Am. Meteorol. Soc.*, *94*, 776–785.

Prasad, A. K., S. Sarkar, R. P. Singh, and M. Kafatos (2007), Inter-annual variability of vegetation cover and rainfall over India, *Adv. Space Res.*, *39*, 79–87.

Propastin, P., L. Fotso, and M. Kappas (2010), Assessment of vegetation vulnerability to ENSO warm events over Africa, *Int. J. Appl. Earth Obs. Geoinformation*, *12*(Supplement 1), S83–S89.

Pulwarty, R. S., and M. V. K. Sivakumar (2014), Information systems in a changing climate: Early warnings and drought risk management, *Weather Clim. Extremes*, *3*, 14–21.

Ray, D. K., J. S. Gerber, G. K. MacDonald, and P. C. West (2015), Climate variation explains a third of global crop yield variability, *Nat. Commun.*, *6*, 5989, doi:10.1038/ncomms6989.

Richard, Y., and I. Poccard (1998), A statistical study of NDVI sensitivity to seasonal and interannual rainfall variations in Southern Africa, *Int. J. Remote Sens.*, *19*, 2907–2920.

Rockel, B., A. Will, and A. Hense (2008), The Regional Climate Model COSMO-CLM (CCLM), *Meteorol. Z.*, *17*, 347–348.

Rodell, M., et al. (2004), The Global Land Data Assimilation System: American Meteorological Society, 85, 381–394, doi:10.1175/BAMS-85-3-381

Roeckner, E., K. Arpe, L. Bengtsson, M. Christoph, M. Claussen, L. Dümenil, M. Esch, M. Giorgetta, U. Schlese, and U. Schulzweida (1996), *The Atmospheric General Circulation Model ECHAM-4: Model Description and Simulation of the Present Day Climate*, Max-Planck-Institut für Meteorologie, Hamburg, Germany.

Roeckner, E., et al. 2003, The atmospheric general circulation model ECHAM5. Part I: Model description, Report No. 349., Hamburg, Germany, Max-Planck-Institut für Meteorologie.

Ropelewski, C. F., and M. S. Halpert (1986), North American precipitation and temperature patterns associated with the El Niño/Southern Oscillation (ENSO), *Mon. Weather Rev.*, *114*, 2352–2362.

Ropelewski, C. F., and M. S. Halpert (1987), Global and regional scale precipitation patterns associated with the El Niño/Southern Oscillation, *Mon. Weather Rev.*, *115*, 1606–1626.

Ropelewski, C. F., and P. D. Jones (1987), An extension of the Tahiti–Darwin Southern Oscillation Index, *Mon. Weather Rev.*, *115*, 2161–2165.

Saji, N. H., B. N. Goswami, P. N. Vinayachandran, and T. Yamagata (1999), A dipole mode in the tropical Indian Ocean, *Nature*, *401*, 360–363.

Sapiano, M. R. P. (2010), An evaluation of high resolution precipitation products at low resolution, *Int. J. Climatol.*, *30*, 1416–1422.

Schlenker, W., and D. B. Lobell (2010), Robust negative impacts of climate change on African agriculture, *Environ. Res. Lett.*, *5*, 8.

Schmidt, M., D. Klein, C. Conrad, S. Dech, and H. Paeth (2014), On the relationship between vegetation and climate in tropical and northern Africa, *Theor. Appl. Climatol.*, *115*, 341–353.

Schreck, C. J., and F. H. M. Semazzi (2004), Variability of the recent climate of eastern Africa, *Int. J. Climatol.*, *24*, 681–701.

Segele, Z. T., L. M. Leslie, and P. J. Lamb (2009), Evaluation and adaptation of a regional climate model for the Horn of Africa: Rainfall climatology and interannual variability, *Int. J. Climatol.*, *29*, 47–65.

Sellers, P. J. (1985), Canopy reflectance, photosynthesis and transpiration, *Int, J. Remote Sens.*, *6*, 1335–1372.

Smith, K. A., and F. H. M. Semazzi (2014), The role of the dominant modes of precipitation variability over eastern Africa in modulating the hydrology of Lake Victoria, *Adv. Meteorol.*, 11, doi:10.1155/2014/516762.

Sorooshian, S., K.-L. Hsu, X. Gao, H. V. Gupta, B. Imam, and D. Braithwaite (2000), Evaluation of PERSIANN system satellite–based estimates of tropical rainfall, *Bull. Am. Meteorol. Soc.*, *81*, 2035–2046.

Spracklen, D. V., S. R. Arnold, and C. M. Taylor (2012), Observations of increased tropical rainfall preceded by air passage over forests, *Nature*, *489*, 282–285.

Steven, M. D., T. J. Malthus, F. Baret, H. Xu, and M. J. Chopping (2003), Intercalibration of vegetation indices from different sensor systems, *Remote Sens. Environ.*, *88*, 412–422.

Sun, L., F. H. M. Semazzi, F. Giorgi, and L. Ogallo (1999), Application of the NCAR Regional Climate Model to eastern Africa: 2. Simulation of interannual variability of short rains, *J. Geophys. Res.*, *104*, 6549–6562, doi:10.1029/1998JD200050.

Swets, D. L., B. C. Reed, J. D. Rowland, and S. E. Marko (1999), A weighted least-squares approach to temporal NDVI smoothing, ASPRS Annual Conference, 17-21 May 1999, p. 526-536.

Swinnen, E. (2008), Vegetation dynamics in Southern Africa from NOAA-AVHRR and SPOT-VGT time series, Ph.D. thesis, Université catholique de Louvain, Louvain-la-Neuve, 208 p.

Swinnen, E., S. Verbeiren, B. Deronde, and P. Henry (2014), Assessment of the impact of the orbital drift of SPOT-VGT1 by comparison with SPOT-VGT2 data, *Int. J. Remote Sens.*, *35*, 2421–2439.

Swinnen, E., and F. Veroustraete (2008), Extending the SPOT-VEGETATION NDVI time series (1998–2006) back in time with NOAA-AVHRR data (1985–1998) for Southern Africa, *IEEE Trans. Geosci. Remote Sens.*, *46*, 558–572.

Taylor, C. M., R. A. M. de Jeu, F. Guichard, P. P. Harris, and W. A. Dorigo (2012), Afternoon rain more likely over drier soils, *Nature*, *489*, 423–426.

Thenkabail, P. S., R. B. Smith, and E. De Pauw (2000), Hyperspectral vegetation indices and their relationships with agricultural crop characteristics, *Remote Sens. Environ.*, *71*, 158–182.

Thiery, W., E. L. Davin, H.-J. Panitz, M. Demuzere, S. Lhermitte, and N. van Lipzig (2015), The impact of the African Great Lakes on the regional climate, *J. Clim.*, *28*, 4061–4085.

Thiery, W., E. L. Davin, S. I. Seneviratne, K. Bedka, S. Lhermitte, and N. P. M. van Lipzig (2016), Hazardous thunderstorm intensification over Lake Victoria, *Nat. Commun.*, *7*, 12786, doi:10.1038/ncomms12786.

Thiery, W., A. Martynov, F. Darchambeau, J. P. Descy, P. D. Plisnier, L. Sushama, and N. P. M. van Lipzig (2014a), Understanding the performance of the FLake model over two African Great Lakes, *Geosci. Model Dev.*, *7*, 317–337.

Thiery, W., et al. (2014b), LakeMIP Kivu: Evaluating the representation of a large, deep tropical lake by a set of one-dimensional lake models, *Tellus A*, *66*, 21390, doi:10.3402/tellusa.v66.21390.

Thornton, P. K., P. G. Jones, G. Alagarswamy, and J. Andresen (2009), Spatial variation of crop yield response to climate change in East Africa, *Global Environ. Change-Human Policy Dimens.*, *19*, 54–65.

Tian, F., R. Fensholt, J. Verbesselt, K. Grogan, S. Horion, and Y. Wang (2015), Evaluating temporal consistency of long-term global NDVI datasets for trend analysis, *Remote Sens. Environ.*, *163*, 326–340.

Torrence, C., and G. P. Compo (1998), A practical guide to wavelet analysis, *Bull. Am. Meteorol. Soc.*, *79*, 61–78.

Tote, C., D. Patricio, H. Boogaard, R. van der Wijngaart, E. Tarnavsky, and C. Funk (2015), Evaluation of satellite rainfall estimates for drought and flood monitoring in Mozambique, *Remote Sens*, *7*, 1758–1776.

Trenberth, K. E. (1997), The definition of El Niño, *Bull. Am. Meteorol. Soc.*, *78*, 2771–2777.

Trenberth, K. E., and D. P. Stepaniak (2001), *Niño Region 3.4 Index, Climate Analysis Section (CAS)*, Clim. Global Dyn. Div., NCAR (National Center for Atmospheric Research), Boulder, Colo.

Trishchenko, A. P., J. Cihlar, and Z. Li (2002), Effects of spectral response function on surface reflectance and NDVI measured with moderate resolution satellite sensors, *Remote Sens. Environ.*, *81*, 1–18.

Tucker, C. J., and P. J. Sellers (1986), Satellite remote sensing of primary production, *Int. J. Remote Sens.*, *7*, 1395–1416.

USGS (1996), *Global 30 Arc-Second Elevation (GTOPO30)*, U.S. Geol. Surv., Reston, Va.

van Leeuwen, W. J., K. Hartfield, M. Miranda, and F. J. Meza (2013), Trends and ENSO/AAO driven variability in NDVI derived productivity and phenology alongside the Andes Mountains, *Remote Sens.*, *5*, 1177–1203.

Verbesselt, J., R. Hyndman, A. Zeileis, and D. Culvenor (2010), Phenological change detection while accounting for abrupt and gradual trends in satellite image time series, *Remote Sens. Environ.*, *114*, 2970–2980.

Wessels, K. J., S. D. Prince, J. Malherbe, J. Small, P. E. Frost, and D. VanZyl (2007), Can human-induced land degradation be distinguished from the effects of rainfall variability? A case study in South Africa, *J. Arid Environ.*, *68*, 271–297.

White, A. B., P. Kumar, and D. Tcheng (2005), A data mining approach for understanding topographic control on climate-induced inter-annual vegetation variability over the United States, *Remote Sens. Environ.*, *98*, 1–20.

Williams, A. P., and C. Funk (2011), A westward extension of the warm pool leads to a westward extension of the Walker circulation, drying eastern Africa, *Clim. Dyn.*, *37*, 2417–2435.

Williams, C. A., and N. P. Hanan (2011), ENSO and IOD teleconnections for African ecosystems: Evidence of destructive interference between climate oscillations, *Biogeosciences*, *8*, 27–40.

Williams, C. A., N. P. Hanan, I. Baker, G. J. Collatz, J. Berry, and A. S. Denning (2008), Interannual variability of photosynthesis across Africa and its attribution, *J. Geophys. Res.*, *113*, G04015, doi:10.1029/2008JG000718.

Wolter, K., and M. S. Timlin (1998), Measuring the strength of ENSO events: How does 1997/98 rank?, *Weather*, *53*, 315–324.

Wolter, K., and M. S. Timlin (2011), El Niño/Southern Oscillation behaviour since 1871 as diagnosed in an extended multivariate ENSO index (MEI.ext), *Int. J. Climatol.*, *31*, 1074–1087.

Wood, S. (2011), Fast stable restricted maximum likelihood and marginal likelihood estimation of semiparametric generalized linear models, *J. R. Stat. Soc.: Series B (Statistical Methodology)*, *73*, 3–36.

Wood, S., and F. Scheipl, (2014), gamm4: Generalized additive mixed models using mgcv and lme4, R package version 0.2-3.

Woodruff, S. D., R. J. Slutz, R. L. Jenne, and P. M. Steurer (1987), A comprehensive ocean-atmosphere data set, *Bull. Am. Meteorol. Soc.*, *68*, 1239–1250.

Wu, Z., and N. E. Huang (2009), Ensemble empirical mode decomposition: A noise-assisted data analysis method, *Adv. Adaptive Data Anal.*, *1*, 1–41.

Xie, P., and P. A. Arkin (1996), Analyses of global monthly precipitation using gauge observations, satellite estimates, and numerical model predictions, *J. Clim.*, *9*, 840–858.

Xie, P., and P. A. Arkin (1997), Global precipitation: A 17-year monthly analysis based on gauge observations, satellite estimates, and numerical model outputs, *Bull. Am. Meteorol. Soc.*, *78*, 2539–2558.

Yang, J., Q. Liu, S.-P. Xie, Z. Liu, and L. Wu (2007), Impact of the Indian Ocean SST basin mode on the Asian summer monsoon, *Geophys. Res. Lett.*, *34*, L02708, doi:10.1029/2006GL028571.

Yengoh, G. T., D. Dent, L. Olsson, A. E. Tengberg, and C. J. Tucker (2014), The use of the normalized difference vegetation index (NDVI) to assess land degradation at multiple scales: A review of the current status, future trends, and practical considerations, Lund University Center for Sustainability Studies (LUCSUS), and the Scientific and Technical Advisory Panel of the Global Environment Facility (STAP/GEF).

Yong, B., Y. Hong, L.-L. Ren, J. J. Gourley, G. J. Huffman, X. Chen, W. Wang, and S. I. Khan (2012), Assessment of evolving TRMM-based multisatellite real-time precipitation estimation methods and their impacts on hydrologic prediction in a high latitude basin, *J. Geophys. Res.*, *117*, D09108, doi:10.1029/2011JD017069.

Zaroug, M. A. H., F. Giorgi, E. Coppola, G. M. Abdo, and E. A. B. Eltahir (2014), Simulating the connections of ENSO and the rainfall regime of East Africa and the upper Blue Nile region using a climate model of the tropics, *Hydrol. Earth Syst. Sci.*, *18*, 4311–4323.

Zhao, Z., J. Gao, Y. Wang, J. Liu, and S. Li (2015), Exploring spatially variable relationships between NDVI and climatic factors in a transition zone using geographically weighted regression, *Theor. Appl. Climatol.*, *120*, 507–519.

Zhou, H., A. Van Rompaey, and J. A. Wang (2009), Detecting the impact of the "Grain for Green" program on the mean annual vegetation cover in the Shaanxi province, China using SPOT-VGT NDVI data, *Land Use Policy*, *26*, 954–960.

Zhou, L., et al. (2014), Widespread decline of Congo rainforest greenness in the past decade, *Nature*, *509*, 86–90.

Zuur, A. F., E. N. Ieno, N. Walker, A. A. Saveliev, and G. M. Smith (2009), *Mixed Effects Models and Extensions in Ecology with R: Statistics for Biology and Health*, Springer, New York.